doi:10.1038/nature12018

Statistical Analysis

Fig 1a. *n* = 5 for each group. p<0.01. Wilcoxon rank-sum test.

Fig. 1b. *n* = 8 for eNpHR3.0:BNST somata group, *n* = 8 for eYFP:BNST somata group. Two-way repeated-measures ANOVA detected significant interaction of group x light-epoch: $F_{2,28}$ = 10.74, p<0.001. Two groups showed significant difference at light-on epoch: p<0.05, post-hoc Bonferroni *t*-test.

Fig. 1d. *n* = 7 for eNpHR3.0:ovBNST group, *n* = 8 for eYFP:ovBNST group. Two-way repeated-measures ANOVA detected significant interaction of group x light-epoch: $F_{2,26}$ = 14.66, p<0.0001. Two groups showed significant difference at light-on epoch: p<0.01, post-hoc Bonferroni *t*-test.

Fig. 1e. *n* = 7 for eNpHR3.0:ovBNST group, *n* = 8 for eYFP:ovBNST group. p<0.05. Wilcoxon rank-sum test.

Fig. 1g. *n* = 11 for eNpHR3.0:BLA-adBNST group, *n* = 15 for eYFP:BLA-adBNST group. Two-way repeated-measures ANOVA detected significant interaction of group x light epoch: $F_{2,48}$ = 5.58, p<0.01. Two groups showed significant difference at light-on epoch: p<0.01, post-hoc Bonferroni *t*-test.

Fig. 1h. *n* = 8 for eNpHR3.0:BLA-adBNST group, *n* = 8 for eYFP:BLA-adBNST group. p<0.01. Wilcoxon rank-sum test.

Fig. 2b. *n* = 11 for ChR2:BLA-adBNST group, *n* = 12 for eYFP:BLA-adBNST group. Two-way repeated-measures ANOVA detected significant interaction of group x light epochs: $F_{2,42}$ = 5.58, p<0.01. Two groups showed significant difference at light-on epoch: p<0.01, post-hoc Bonferroni *t*-test.

Fig. 2c. *n* = 7 for ChR2:BLA-adBNST group, *n* = 8 for eYFP:BLA-adBNST group. p<0.05. Wilcoxon rank-sum test.

Fig. 2d. *n* = 8 for ChR2:BLA-adBNST group, *n* = 6 for eYFP:BLA-adBNST group. p>0.05. Wilcoxon rank-sum test.

Fig. 2f. *n* = 11 for ChR2:adBNST-LH group, *n* = 8 for eYFP:adBNST-LH group. Two-way repeated-measures ANOVA detected significant interaction of group x light epochs: $F_{2,34}$ = 8.51, p = 0.0010. Two groups showed significant difference at light-on epoch: p<0.001, post-hoc Bonferroni *t*-test.

Fig. 2g. *n* = 9 for ChR2:adBNST-LH group, *n* = 10 for eYFP:adBNST-LH group. p>0.05. Wilcoxon rank-sum test.

Fig. 2h. *n* = 7 for ChR2:adBNST-LH group, *n* = 7 for eYFP:adBNST-LH group. p>0.05. Wilcoxon rank-sum test.

Fig. 2j. *n* = 7 for ChR2:BNST-PB group, *n* = 7 for eYFP:BNST-PB group. Two-way repeated-measures ANOVA failed to detect a significant interaction of group x light epoch: p>0.05.

Fig. 2k. *n* = 8 for ChR2:BNST-PB group, *n* = 7 for eYFP:BNST-PB group. p<0.05. Wilcoxon rank-sum test.

Fig. 2l. *n* = 7 for ChR2:BNST-PB group, *n* = 5 for eYFP:BNST-PB group. p>0.05. Wilcoxon rank-sum test.

Fig. 2m. *n* = 7 for ChR2:adBNST-VTA group, *n* = 7 for eYFP:adBNST-VTA group. Two-way repeated-measures ANOVA failed to detect a significant interaction of group x light epoch: p>0.05.

Fig. 2o. *n* = 8 for ChR2:adBNST-VTA group, *n* = 7 for eYFP:adBNST-VTA group. p>0.05. Wilcoxon rank-sum test.

Fig. 2p. *n* = 8 for ChR2:adBNST-VTA group, *n* = 7 for eYFP:adBNST-VTA group. p<0.001. Wilcoxon rank-sum test.

Fig. 3c. *n* = 55 adBNST single units.

Fig. 3f. *n* = 19 adBNST neurons.

Fig. 3l. *n* = 14 adBNST neurons.

Fig. 4f. *n* = 38 adBNST single units. Spearman's rho = 0.57, p < 0.0001.

Fig. 4g. *n* = 38 adBNST single units. EPM score in light-on epoch was smaller than EPM score in light-off epoch: p<0.05, Wilcoxon rank-sum test. EPM score generated from jittered spikes was smaller than EPM scores in light-on and -off epochs: p<0.001 for both, Wilcoxon rank-sum test.

Supplementary Fig. 5a. *n* = 10 for eNpHR3.0:BNST somata group, *n* = 11 for eYFP:BNST somata group. Two-way repeated-measures ANOVA did not detect significant interaction of group x light epoch. **(Inset)** Two-way repeated-measures ANOVA detected significant interaction of group x light epoch: $F_{1,13}$ = 8.34, p<0.05. Two

groups showed a significant difference in the light-on epoch: $p<0.05$, post-hoc Bonferroni *t*-test.

Supplementary Fig. 5b. n = 10 for eNpHR3.0:BNST somata group, n = 11 for eYFP:BNST somata group. Two-way repeated-measures ANOVA detected significant interaction of group x light epoch: $F_{2,26} = 4.70$, $p<0.05$. Two groups showed a significant difference in the light-on epoch: $p<0.05$, post-hoc Bonferroni *t*-test.

Supplementary Fig. 5c. n = 7 for eNpHR3.0:ovBNST group, n = 8 for eYFP:ovBNST group. Two-way repeated-measures ANOVA detected significant interaction of group x light epoch: $F_{3,42} = 7.93$, $p<0.001$. **(Inset)** Two-way repeated-measures ANOVA detected significant interaction of group x light epoch: $F_{1,14} = 31.03$, $p<0.05$. Two groups showed a significant difference in the light-on epoch: $p<0.05$, post-hoc Bonferroni *t*-test.

Supplementary Fig. 5d. n = 7 for eNpHR3.0:ovBNST group, n = 8 for eYFP:ovBNST group. Two-way repeated-measures ANOVA detected significant interaction of group x light epoch: $F_{2,26} = 6.67$, $p<0.01$. Two groups showed a significant difference in the light-on epoch: $p<0.01$, post-hoc Bonferroni *t*-test.

Supplementary Fig. 5e. n = 13 for eNpHR3.0:BLA-adBNST group, n = 15 for eYFP:BLA-adBNST group. Two-way repeated-measures ANOVA detected significant interaction of group x light epoch: $F_{3,78} = 4.35$, $p<0.01$. **(Inset)** Two-way repeated-measures ANOVA detected significant interaction of group x light epoch: $F_{1,26} = 12.56$, $p<0.01$. Two groups showed a significant difference in the light-on epoch: $p<0.05$, post-hoc Bonferroni *t*-test.

Supplementary Fig. 5f. n = 13 for eNpHR3.0:BLA-adBNST group, n = 15 for eYFP:BLA-adBNST group. Two-way repeated measures ANOVA detected significant interaction of group x light epoch: $F_{2,48} = 6.24$, $p<0.01$. Two groups showed a significant difference in the light-on epoch: $p<0.001$, post-hoc Bonferroni *t*-test.

Supplementary Fig. 9a. n = 11 for ChR2:BLA-adBNST group, n = 11 for eYFP:BLA-adBNST group. Two-way repeated measures ANOVA detected significant interaction of group x light epoch: $F_{3,60} = 2.89$, $p<0.05$. Two groups showed significant difference at the first light-on epoch: $p<0.05$, post-hoc Bonferroni *t*-test. **(Inset)** Two-way repeated-measures ANOVA detected significant interaction of group x light epoch: $F_{1,20} = 9.72$,

p<0.01. Two groups showed significant a difference in the light-on epoch: p<0.05, post-hoc Bonferroni *t*-test.

Supplementary Fig. 9b. *n* = 11 for ChR2:BLA-adBNST group, *n* = 11 for eYFP:BLA-adBNST group. Two-way repeated-measures ANOVA detected significant interaction of group x light epoch: $F_{2,42}$ = 4.21, p<0.05. Two groups showed a significant difference in the light-on epoch: p<0.01, post-hoc Bonferroni *t*-test.

Supplementary Fig. 9c. *n* = 11 for ChR2:adBNST-LH group, *n* = 8 for eYFP:adBNST-LH group. Two-way repeated-measures ANOVA did not detect a significant interaction of group x light epoch. **(Inset)** However, when light-off and light-on epochs were averaged, two-way repeated measures ANOVA detected significant interaction of group x light epoch: $F_{1,17}$ = 5.59, p<0.05. Two groups showed a significant difference in the light-on epoch: p<0.001, post-hoc Bonferroni *t*-test.

Supplementary Fig. 9d. *n* = 11 for ChR2:adBNST-LH group, *n* = 8 for eYFP:adBNST-LH group. Two-way repeated-measures ANOVA detected a significant interaction of group x light epoch: $F_{2,34}$ = 4.41, p<0.05. Two groups showed a significant difference in the light-on epoch: p<0.001, post-hoc Bonferroni *t*-test.

Supplementary Fig. 9e. *n* = 7 for ChR2:BNST-PB group, *n* = 7 for eYFP:BNST-PB group. Two-way repeated-measures ANOVA failed to detect a significant interaction of group x light epoch: p>0.05. **(Inset)** Two-way repeated-measures ANOVA failed to detect significant interaction of group x light epoch: p>0.05.

Supplementary Fig. 9f. *n* = 7 for ChR2:BNST-PB group, *n* = 7 for eYFP:BNST-PB group. Two-way repeated-measures ANOVA failed to detect a significant interaction of group x light epoch: p>0.05.

Supplementary Fig. 6g. *n* = 8 for ChR2:adBNST-VTA group, *n* = 7 for eYFP:adBNST-VTA group. Two-way repeated-measures ANOVA failed to detect a significant interaction of group x light epoch: p>0.05. **(Inset)** Two-way repeated-measures ANOVA failed to detect a significant interaction of group x light epoch: p>0.05.

Supplementary Fig. 9h. *n* = 8 for ChR2:adBNST-VTA group, *n* = 7 for eYFP:adBNST-VTA group. Two-way repeated-measures ANOVA failed to detect a significant interaction of group x light epoch: p>0.05.

Supplementary Fig. 14a. Chi-square test detected significant differences between: (1)-(2) ($\chi^2(1, n=347)=19.132$, p<0.0001), (1)-(3) ($\chi^2(1, n= 376)=29.567$, p<0.0001) and (1)-(4) ($\chi^2(1, n= 215)=17.287$, p<0.0001).

Supplementary Fig. 17f-i. *n* for each condition is listed in the table below.

Condition	*n* (number of cells actived after stimulation)	*n* (all cells)
0 μA	37	220
10 μA	109	370
20 μA	127	370
30 μA	130	369
40 μA	129	372
50 μA	148	371
APV	61	277
NBQX+APV	59	279

Supplementary Fig. 17f. Chi-square test detected significant differences between: 0 μA-50 μA ($\chi^2(1, n=220)=49.26$, p<0.0001), 50 μA-APV ($\chi^2(1, n=277)=37.31$, p<0.0001) and 50 μA-NBQX+APV ($\chi^2(1, n=279)=41.32$, p<0.0001),

Supplementary Fig. 17g. One-way ANOVA detected significant main effect of stimulation condition: $F_{7,792} = 8.512$, p<0.001. Post-hoc Tukey's test revealed significant differences between: 0 μA-50 μA (p=0.001), 10 μA-30 μA (p=0.019), 10 μA-40 μA (p=0.001), 10 μA-50 μA (p<0.001), 10 μA-APV (p=0.001), 10 μA-NBQX+APV (p=0.003), 20 μA-50 μA (p<0.001) and 30 μA-50 μA (p=0.022).

Supplementary Fig. 17h. *n* = 137 adBNST neurons. Spearman's rho and p values:

Condition	*n*	Spearman's rho	p
0 μA	84	-0.2542	0.1289
10 μA	96	-0.1326	0.1692
20 μA	119	0.12	0.1791
30 μA	133	0.3901	4.48×10^{-6}
40 μA	126	0.457	5.22×10^{-8}
50 μA	137	0.5729	2.76×10^{-14}

Supplementary Fig. 17i. One-way ANOVA detected significant main effect of stimulation condition: $F_{7,792}$ = 2.222, p=0.031. Post-hoc Tukey's test failed to detect significant differences between conditions.

Materials and Methods

Subjects

Male C57BL/6 mice, aged 6-8 weeks at the start of experiments, were housed in a reverse 12-hr light/dark cycle. Food and water were given *ad libitum*. Dopamine receptor D1a (Drd1a)-Cre transgenic mice (founder line: EY266) were obtained from GENSAT. All mice used for behavioral experiments were single-housed to reduce baseline behavioral variability, except for eNpHR3.0:BLA-adBNST and ChR2:BNST somata mice, which were group-housed to decrease baseline anxiety levels[1]. In addition, a cohort of ChR2:BLA-adBNST mice (used to produce data presented in Fig. 2d and Supplementary Fig. 10) was group housed to demonstrate that stimulation of the BLA-adBNST projection is anxiolytic in group-housed, low-anxiety-baseline animals. All experimental protocols were approved by the Stanford University Institutional Animal Care and Use Committee and were in accordance with the guidelines from the National Institute of Health.

Virus production

The adeno-associated virus (AAV) vectors were serotyped with AAV5 coat proteins and packaged by the University of North Carolina Vector Core (Chapel Hill, NC, USA). Viral titers were:

- 4x 10^{12} particles / ml for AAV5:CaMKIIα::hChR2(H134R)-eYFP
- 3 x 10^{12} particles / ml for AAV5:CaMKIIα::eYFP
- 4 x 10^{12} particles / ml for AAV5:CaMKIIα::eNpHR3.0-eYFP
- 4 x 10^{12} particles / ml for AAV5:hSyn::hChR2(H134R)-eYFP
- 4 x 10^{12} particles / ml for AAV5:hSyn::eYFP
- 4 x 10^{12} particles / ml for AAV5:hSyn::eNpHR3.0-eYFP
- 2 x 10^{12} particles / ml for AAV5:EF1α::DIO-eNpHR3.0-eYFP
- 2 x 10^{12} particles / ml for AAV5:EF1α::DIO-ChR2(H134R)-eYFP

The maps for these constructs are available at www.optogenetics.org. The herpes simplex virus (HSV) was derived by R.N. from HSV strain 17+ and was replication-incompetent. The functional titer of this HSV amplicon virus, which enables persistent expression in vivo, was 3 x 10^8 infectious units (i.u.) / ml. Rabies virus (RV) was produced by B.K.L. and R.C.M. as previously described[2]. Rabies virus glycoprotein (RVG) was replaced by eGFP or tdTomato to generate virus expressing eGFP (RV:eGFP) or tdTomato (RV:tdTomato).

Stereotactic viral injection and guide cannula/fiberoptic cannula implantation

All surgical procedures were performed aseptically. Mice were anaesthetized with 1.5-3.0% isoflurane, and were placed in a stereotaxic apparatus (Kopf Instruments, Tujunga, CA, USA) while resting on a heating pad. For mice used in drug injection experiments, a small craniotomy was performed, and a guide cannula (22 gauge C313G/SPC GUIDE 38172; PlasticsOne, Roanoke, VA, USA) was unilaterally placed on top of the BNST (AP +0.2 mm, ML1.0 mm, DV-3.9 mm). All coordinates are relative to bregma in mm[3]. Adhesive cement (C&B metabond; Parkell, Edgewood, NY, USA) was first applied and dental cement (Stoelting, Wood Dale, IL, USA) was added to secure the cannula to the skull. The incision was closed using tissue adhesive (Vetbond; Fisher, Pittsburgh, PA, USA). A dummy cap (C313DC/1/SPC DUMMY .014/.36MM; PlasticsOne) was inserted to maintain the cannula guide free of obstructions.

For all mice used in behavioral optogenetic manipulations, 0.5 µl of virus was injected per site. ChR2 mice received unilateral viral infusion and fiberoptic cannula implantation (0.22 NA, 200 µm diameter; Doric Lenses, Quebec, Canada), whereas all eNpHR3.0 mice were bilaterally injected and implanted since unilateral loss-of-function may be compensated by the other hemisphere. All unilateral manipulations including drug injection, viral injection and cannula implantation were counter-balanced across hemispheres. For optogenetic manipulations of BNST somata, after a small craniotomy, AAV5:hSyn::eNpHR3.0-eYFP or AAV5:hSyn::ChR2-eYFP was injected in the center of the dorsal BNST (AP +0.2 mm, ML ±1.0 mm, DV -4.3 mm) using a 10 µl syringe and a

33 gauge beveled metal needle (Nanofil, WPI, Sarasota, FL, USA), with the bevel facing anteriorly. hSyn (human synapsin) is a pan-neuronal promoter[4] which enables expression of transgenes in all neurons in the BNST. Injections were via syringe pump (UMP3; WPI) and rate was set to 0.1 µl/min by the controller (Micro4; WPI). After injection the needle was slowly lifted 100 µm, and then left in place for 5 additional minutes before slow withdrawal to avoid upward flow of the liquid along the needle. Control groups were injected with AAV5:hSyn::eYFP. Two fiberoptic cannulae were then placed on top of the bilateral BNST (AP +0.2 mm, ML 1.0 mm, DV -4.0 mm) and secured to the skull as described above. Mice recovered from anesthesia in a warm cage. Behavioral and electrophysiological experiments were conducted within a window of 4-6 weeks (for all cell body manipulations) or 8-12 weeks (for all terminal manipulations) after injection, to allow for opsin expression.

For optogenetic stimulations of BNST terminals in the LH, PB or VTA, all procedures were the same, except that AAV5:hSyn::ChR2-eYFP was delivered into the BNST and fiberoptic cannulae were placed above the LH (AP -1.0 mm, ML 1.3mm, DV -5.0 mm), PB (AP -5.2 mm, ML 1.5 mm, DV -3.2 mm) or VTA (AP -3.4 mm, ML 0.3 mm, DV -3.9 mm). For optogenetic manipulations of BLA terminals in the BNST, AAV:CaMKIIα::hChR2(H134R)-eYFP, AAV:CaMKIIα::eNpHR3.0-eYFP or (for control) AAV:CaMKIIα::eYFP was delivered into the BLA (AP -1.6 mm, ML ± 3.1mm, DV -4.9 mm) and fiberoptic cannulae were placed on top of the BNST. As CaMKIIα is a marker of glutamatergic pyramidal neurons in the BLA[5], the use of the CaMKIIα promoter enables transgene expression favoring BLA pyramidal neurons. To stimulate BLA fibers in the anterior commissure, AAV:CaMKIIα::hChR2(H134R)-eYFP was injected to the BLA and the fiberoptic cannula was implanted right above the anterior commissure (AP +0.14 mm, ML 1.5 mm, DV -4.4 mm). For optogenetic inhibition of the ovBNST, Drd1a-Cre mice were injected with AAV:EF1α::DIO-eNpHR3.0-eYFP on top of the BNST and fiberoptic cannulae were placed on top of the BNST.

For probing the regions projecting to the ovBNST, 0.3 µl of RV:eGFP was injected in the ovBNST (AP +0.2 mm, ML 1.0 mm, DV -4.1 mm). For dual rabies virus injections, 0.5 µl of RV:eGFP, 0.5 µl of RV:tdTomato or 0.5 µl of the mixture of two viruses were injected

in the LH (AP -1.5 mm, ML 1.0 mm, DV -5.6 mm), PB (AP -5.2 mm, ML 1.0 mm, DV -3.8 mm) or VTA (AP -3.5 mm, ML 0.35 mm, DV -4.5 mm).

Drug delivery

For the glutamate receptor antagonist infusion in the BNST, a glutamate antagonist solution consisting of 10 mM 2,3-dihydroxy-6-nitro-7-sulfamoyl-benzo[f]quinoxaline-2,3-dione (NBQX; Tocris, Ellisville MO, USA) and 50 mM 2-amino-5-phosphonopentanoic acid (D-APV; Tocris) was dissolved in saline (0.9% NaCl). Thirty minutes before the anxiety assays, 0.3 µl of the glutamate antagonist solution was infused in the BNST via an internal infusion needle (28 gauge C313I/SPC INTERNAL38799; PlasticsOne), inserted into the same guide cannula used to introduce fiberoptic cannulae for light delivery. The internal needle was connected to a 10-µl Hamilton syringe (Nanofil; WPI). The flow rate (0.1 µl/min) was regulated by a syringe pump (Harvard Apparatus, Holliston, MA, USA). The internal infusion needle protruded beyond the cannula guide by ~500 µm, to penetrate potential blood-clotting at the tip of the cannula guide and reach the center of the dorsal BNST. The infusion needle was removed 2 min following the termination of the injection to avoid spillage from the guide cannula.

Light delivery

For all optogenetic inhibition experiments using eNpHR3.0, 5 mW (159 mW/mm^2 at the tip of the fiberoptic) of yellow light was generated by a 593.5 nm DPSS laser (MGL-F593.5; OEM Laser Systems, East Lansing, MI, USA), and bilaterally delivered to mice through two fiberoptic patch cords (0.22 NA, 200 µm diameter; Doric Lenses) that were attached to the implanted fiberoptic cannulae, using a connecting plastic sleeve. For all optogenetic stimulation experiments using ChR2, 3-5 mW of blue light (95-159 mW/mm^2 at the tip of the fiberoptic) was generated by 473 nm DPSS laser (MBL-III473; OEM Laser Systems) and unilaterally delivered. Constant yellow laser was used for yellow light delivery to all eNpHR3.0 mice, while blue laser output was controlled using

a pulse generator (Master-8; AMPI, Jerusalem, Israel) to deliver 5-ms light pulse trains at 10 Hz (for all ChR2 mice except for ChR2:adBNST-VTA mice) or at 20 Hz (for ChR2:adBNST-VTA mice).

Behavioral assays

All mice were handled for three days before behavioral assays for 5 min per day to reduce stress introduced by contact with experimenter. 1-5 minutes were allowed for recovery in the home cage from handling for connecting the fiberoptic cannula and patchcord, before the session was initiated. The elevated plus maze was made of plastic and consisted of two gray open arms (30 × 5 cm) and two grey enclosed arms (30 × 5 × 30 cm) extending from a central platform (5 × 5 × 5 cm) at 90 degrees in the form of a plus. Arms of the same type faced each other. The maze was placed 30 cm above the floor. Mice were individually placed in the center, with the head facing a closed arm. The elevated plus maze test consisted of a 15-min session divided into three 5-min epochs: the pre-stimulation light-off epoch, the light-on epoch and the post-stimulation light-off epoch, in order (off-on-off epochs). The open-field chamber (50 × 50 cm) was made of plastic and was divided into a central field (center, 25 × 25 cm) and an outer field (periphery). Individual mice were placed in the periphery of the field at the start of the test. The open field test consisted of a 20 min session in which there were four 5 min epochs (off-on-off-on epochs). The epochs alternated between no light and light stimulation periods, beginning with the baseline light-off epoch. For all analyses and plots where only light-off and -on conditions are displayed, both off epochs were pooled and both on epochs were pooled. Real-time place preference test was performed in a custom-made black plastic arena (50 x 50 x 25 cm) consisting of two indistinguishable chambers for 15 min. One chamber was paired with light stimulation. The choice of paired chamber was counterbalanced across mice. Animals were placed in the unstimulated chamber at the start of the session and received light stimulation initiated upon every entry into the paired chamber. Light-dark box test was performed in a custom-made grey plastic arena (50 x 25 cm) consisting of light and dark

compartments for 15 min. The mouse was placed in the dark compartment at the beginning of the experiment. For all behavior assays, video tracking software (Viewer^2; BIOBSERVE, St. Augustin, Germany) was used to automatically track location and velocity.

Respiratory rate and heart rate measurement

Respiratory rate and heart rate were measured with a pulse oximeter (MouseOx Plus; Starr Life Sciences, Allison Park, PA, USA) connected to a computer equipped with MouseOx Plus software. For recordings from awake mice, a collar sensor was used. Mice were shaved around the neck and acclimated to the collar sensor (Starr Life Sciences, Allison Park, PA, USA) overnight. Additionally, mice were habituated to handling by the experimenter for three days prior to the measurements. All recordings were made on top of the cage, unless otherwise stated. Mice were given 5 min for acclimation on the cage and were recorded for 3 min as the baseline measurement, and light was delivered for the next 3 min. Respiratory rate as a moving average of 10 measurements was obtained every 1.7 seconds. Heart rate was recorded as a moving average over 5 heart beats. Recording was often discontinued due to signal loss or motion artifacts; therefore, all parameters were carefully monitored in real time and recordings were discarded when physiologically unrealistic values were observed due to insufficient sampling (e.g. respiratory rate of < 100 brpm or heart rate of < 600 bpm). To ensure the quality of the recording, at least two recordings per mouse were made and averaged, and recordings that failed to monitor heart and respiration rates for more than 30% of time were discarded. All respiratory rate data were obtained with the protocol described above, except for data shown in Supplementary Figs. 8 and 13. The procedure used in these figures is detailed below.

To compare respiratory rates between the home cage and the open field, respiration rates were measured in these two environments in the same mice. Mice were recorded in the home cage or the open field for 3 min, given 5 min for recovery in a new clean cage and then recorded in the other environment for 3 min. Recordings were started

immediately after placing the mice in each environment. To counterbalance the order of recording, in half of the mice, the recording was performed in the home cage first and then in the open field (Group A, in the figure below). For the other half, the order of recording was switched (Group B). Between two recordings, each mouse was allowed to recover in a new, clean cage. The data shown in Supplementary Fig. 7 was recorded according to the scheme below:

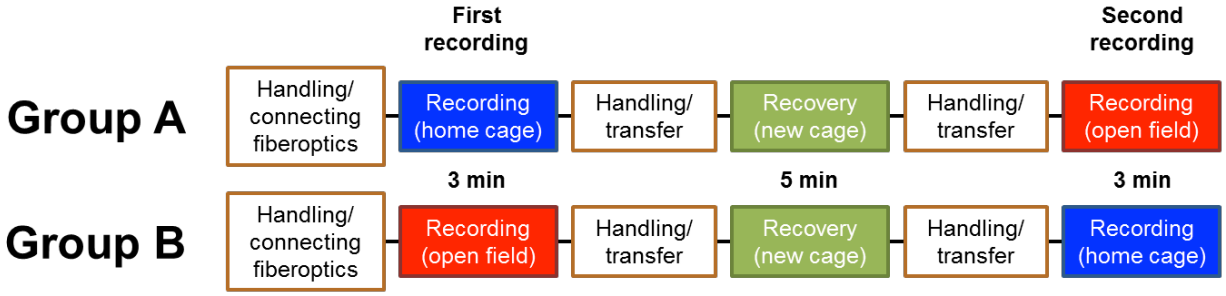

Respiratory rates from the open field were divided by respiratory rates from the home cage and the resulting value was compared between the ChR2 and eYFP groups. Thus, respiratory rates in the home cage were used as the baseline for all mice, both in group A and B. Handling and transporting mice across environments was done both before recording in the home cage and before recording in the open field. Therefore, handling itself could not underlie differences in respiratory rate between environments (moreover, all animals were extensively handled three days prior to the recordings to habituate animals both to handling and to moving with the collar sensor clipped on). To further demonstrate that handling and transferring mice across environments cannot be responsible for the observed effect, we compared respiratory rates of Group A in the open field with Group B in the home cage. Even though both groups of mice were equally handled/transported prior to the recording, mice placed in the open field exhibited statistically significant higher respiratory rates than the ones in the home cage (233.1 ± 12.8 brpm, n = 3 for the open field; 170.3 ± 7.4 brpm, n = 4 for the home cage; $p<0.05$), showing that increased respiratory rate is caused by the open field and cannot be attributed to prior transportation and handling. For the experiment shown in Supplementary Fig. 13, light was delivered when mice were placed in the open field. The protocol used to obtain the data shown on Supplementary Fig. 13 was identical to

that used in Supplementary Fig. 7, with the difference that blue light was delivered during exploration of the open field, as shown in the scheme below.

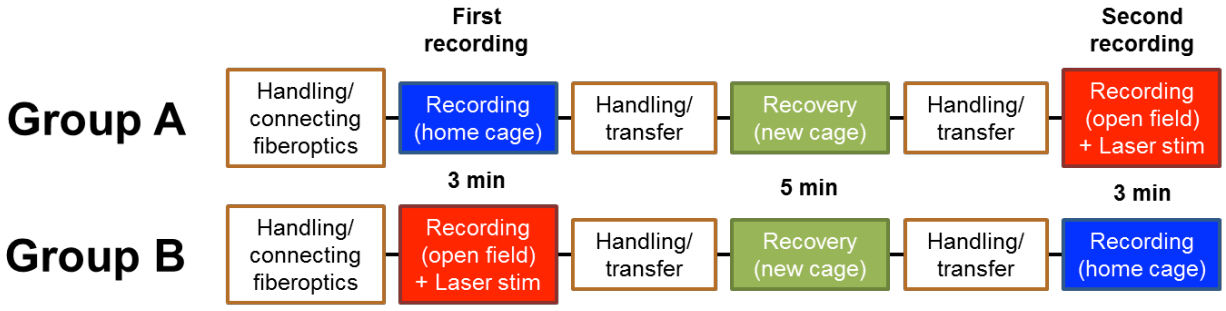

Ex vivo electrophysiological recording

For slice physiology in combination with optogenetics, 3-4 week old male wild-type mice were injected with AAV-CaMKIIα::ChR2-eYFP into the BLA, or male Drd1a-Cre mice were injected with AAV-EF1α::DIO-ChR2(H134R)-eYFP into the ovBNST. After a month, acute 300 μm coronal slices were obtained by transcardially perfusing ice-cold sucrose cutting solution (in mM; 11 D-glucose, 234 sucrose, 2.5 KCl, 1.25 NaH_2PO_4, 10 $MgSO_4$, 0.5 $CaCl_2$, 26 $NaHCO_3$) and slicing in the same solution using a vibratome (VT1000S; Leica, Buffalo Grove, IL, USA). Slices were recovered in oxygenated artificial cerebrospinal fluid (aCSF; in mM, 123 NaCl, 26 $NaHCO_3$, 3 KCl, 1.25 NaH_2PO_4, 1 $MgCl_2$, 2 $CaCl_2$, and 11 glucose) at 32°C for one hour. All electrophysiological recordings were made under the constant perfusion of aCSF bubbled with 95% O_2/5% CO_2 and heated to 32°C. Neurons were visualized with an upright microscope (DM-LFSA; Leica) equipped with both DIC optics and a filter set for visualizing eYFP, using a 40x water-immersion objective and a charge-coupled device (CCD) camera (RetigaExi FAST; QImaging, Surrey, Canada). Slices containing the BLA were used to verify the expression of ChR2 in the BLA, and only the slices from the mice with ChR2 expression restricted to the BLA were used. Whole-cell recordings were made from adBNST neurons (see further discussion below), using patch electrodes (3-6 MΩ) filled with either potassium-based internal solution (in mM; 10 HEPES, 4 Mg-ATP, 0.5 $MgCl_2$, 0.4 Na_3-GTP, 10 NaCl, 0.5 EGTA and 140 potassium gluconate) or cesium-based internal

solution (in mM; 10 HEPES, 4 Mg-ATP, 0.3 Na_3-GTP, 2 NaCl, 8 CsCl, 4 EGTA, 1 QX-314 and 130 cesium gluconate). Most voltage-clamp experiments and all current-clamp experiments were conducted with potassium-based internal solution, and some voltage-clamp experiments were done with cesium-based internal solution to improve spatial clamp. Series resistances were typically 10-20 MΩ.

For the blue light delivery, light was emitted from a 300 W broad-wavelength xenon lamp source (DG-4, Sutter Instruments, Novato, CA, USA), band-pass filtered at 470 ± 20 nm (Semrock; Rochester, NY, USA), passed through additional neutral density filters (ThorLabs; Newton, NJ, USA) and coupled to the fluorescence port of the microscope. For all experiments, 5-15 mW/mm^2 of light was delivered to slices through 40x, 0.8 NA objectives. Pulsed input signals were generated from pClamp (Molecular Devices; Sunnyvale, CA, USA) and were delivered to the DG-4 via BNC.

Voltage-clamp recordings were made at both -70 mV to isolate EPSCs, and at 0 mV to isolate IPSCs. Light-evoked EPSCs and IPSCs were abolished by bath application of glutamate receptor antagonists (10 μM NBQX and 50 μM APV; *n* = 4; Supplementary Fig. 16e). IPSCs were confirmed via bath application of 100 μM picrotoxin (10 μM; *n* = 4; Supplementary Fig. 16f), respectively. We also performed current-clamp recordings when the cell was resting at approximately -60 mV. Currents were filtered at 2 kHz, digitized at 50 kHz, and recorded to disk using pClamp10 software (Molecular Devices).

For the experiments stimulating BLA axon fibers, patch-clamp recordings were from the adBNST. Although there is no clear anatomical boundary between the ovBNST and the adBNST seen with DIC optics, we conducted recordings in the region where eYFP-expressing fibers were present as the ovBNST does not receive projections from the BLA (Fig. 1f and 2a, also see Dong *et al.*, 2001[6]). In agreement with this, putative ovBNST neurons in the dorsal region of the BNST did not exhibit any light-evoked responses (data not shown). For the experiments recording from adBNST neurons projecting to the LH, HSV:EF1α::GFP was injected into the LH (AP -1.5 mm, ML 1.2 mm, DV -6.0 mm) 3-4 days before slice physiology experiments to label adBNST neurons

projecting to the LH. Patch-clamp recordings were performed in GFP-expressing BNST neurons after visually identifying GFP expression in individual cells.

Microdrive construction and implantation

Custom microdrives containing eight stereotrodes surrounding a fiberoptic cannula (0.22 NA, 200 μm diameter; Doric Lenses) were constructed based on interface boards (EIB-16; Neuralynx; Bozeman, MT, USA) attached to a Teflon platform (modified from Adhikari *et al.*, 2011[7]). Stereotrodes were constructed of 25 mM Formvar-coated tungsten microwires (M165260; California Fine Wire; Grover Beach, CA, USA) and were secured to a cannula attached to the interface board. A fiberoptic cannula was attached to the interface board and glued to the microwires in such a way that microwires protruded beyond the tip of the optic fiber by ~0.5 mm. The whole platform was fastened to Teflon cuffs via three fine machine screws (SHCX-080-6; Small Parts; Miramar, FL, USA), allowing the platform to advance by turning the screws into the cuffs. For implantation, additional screws were implanted on the posterior and anterior portions of the skull to serve as ground and physical support, respectively. After carefully placing the microdrive in the BNST, the Teflon cuffs were cemented to the skull (Grip Dental Cement; Dentsply, York, PA, USA), and the ground screw was connected to the interface board.

***In vivo* single-unit recordings**

Animals were permitted to recover for at least one week, and then food-restricted to 85% body weight. During food-restriction, animals were familiarized to the recording setup and handling by being tethered to the head stage in their home cages. The EPM was chosen for the *in vivo* recording over the OFT, because it has well-defined boundaries between the more anxiogenic (open arms) and the safe areas (closed arms). Furthermore, typically mice explore the entire EPM, while most of the area of the center of the OFT is not visited. This increases the accuracy in the estimation of firing rates in

each arm of the EPM. As an independent assay of anxiety, the light-dark box test was performed in a custom-made grey plastic arena (50 x 25 cm) consisting of light and dark compartments for 15 min. Mice were placed in the dark compartment at the beginning of the experiment.

Stereotrodes were advanced until at least four well-isolated single units could be recorded in the BNST. Activation or inhibition of the ChR2- or eNpHR3.0-expressing BLA fibers respectively increased or decreased activity in the recorded area. This indicates that recording was in the adBNST, as light delivery would not be expected to change activity in the ovBNST which lacks BLA fibers. Furthermore, electrical lesions made to mark the tip of the electrodes were only observed in the adBNST (Supplementary Fig. 2). Recordings were obtained via a unitary gain head-stage preamplifier (HS-16; Neuralynx; Bozeman, MT, USA) attached to a fine wire cable. Spikes exceeding 40 μV were band-pass filtered (600–6,000 Hz) and recorded at 32 kHz. Spike data were acquired with Cheetah data acquisition software (Neuralynx). Animal position was obtained by overhead video tracking (30 Hz) of two light-emitting diodes affixed to the headstage.

Single-unit spike sorting and analysis

Data were imported into Matlab for analysis using custom-written software. Clustering of spikes was performed offline manually with SpikeSort 3D (Neuralynx). To classify the *in vivo* response of adBNST single units to stimulation of ChR2-expressing BLA terminals, we recorded responses across 400 presentations of a 5-ms blue light pulse. Firing rates were analyzed in a 100 ms epoch centered at the laser pulse onset (-50 to 50 ms, with the pulse occurring at 0 ms). If z-scored firing rates were significantly different between baseline (-50 to 0 ms) and after the pulse (0 to 35 ms), units were classified as "responsive" to the pulse. Among "responsive units", if the z-scored mean firing rate was higher after the pulse, units were classified as "significantly excited". Otherwise, they were classified as inhibited. Excited units were further divided into units exhibiting

"only transient responses" (firing rates from 0 to 10 ms significantly higher than baseline and rates from 10 to 35 ms not significantly different from baseline) or units exhibiting "transient and sustained responses" (rates from 0 to 35 ms after onset are significantly higher than baseline rates). Persistent multiunit activity was defined as firing rates (measured as z-scores) significantly higher in the seconds 30 to 40 compared to baseline (seconds -30 to 0). Wilcoxon rank-sum test was used to compare responses to the laser pulse.

EPM score calculation

Only data from mice that explored all arms of the maze were used. EPM scores were computed to quantify the extent to which single units can consistently differentiate the open arm vs. closed arm structure of the maze[7]. EPM scores were calculated through the following formula as previously described[7]:

$$\text{Score} = (A - B) / (A + B), \text{ where}$$

$$A = 0.25 \times (| F_L - F_U | + | F_L - F_D | + | F_R - F_U | + | F_R - F_D |) \text{ and}$$

$$B = 0.5 \times (| F_L - F_R | + | F_U - F_D |).$$

F_L, F_R, F_U, and F_D are the % difference from mean firing rate in left, right, up and down arms, respectively. "A" is the mean difference in normalized firing rate between arms of different types, while "B" is the mean difference for arms of the same type. Although we used rates in each location as "% change from mean firing rate", one could also use "fold-increase from mean firing rate", as this choice does not affect the final EPM score. Cells with firing patterns related to the task have similar firing rates in arms of the same type (resulting in a small B) and large differences in rates between arms of different types (resulting in a large value for A). Importantly, a positive score would be assigned both to a cell that fires selectively in both open arms, as well as to a cell that fires selectively in both closed arms. The maximum score of 1.0 indicates no difference in firing rates across arms of the same type (B = 0). On the other hand, a score of zero

would be assigned to the cell that has the same firing rate in all arms of the maze. Lastly, negative scores indicate that firing rates are more similar across arms of different types than across arms of the same type (e.g. the cell that has high firing rates selectively in only one closed arm and one open arm).

To calculate EPM scores during the light OFF epoch, all spikes from a given single unit during the 10 OFF epochs were pooled together. Each epoch has 60 seconds (see Fig. 4e). The total number of spikes in the OFF epoch divided by the total number of seconds in the OFF epoch (60 sec/epochs × 10 epochs = 600 sec) yielded the mean firing rate in the OFF epoch. Firing rates in each arm were calculated as % change from this mean OFF firing rate. These firing rates were used to calculate the OFF EPM scores, as shown in the formula above.

Analogously, to calculate EPM scores during the light ON epoch, all the spikes from a given single unit that occurred in the ON epoch were pooled together to calculate the mean ON firing rate. Note that spiking activity in the OFF epoch has no influence on the calculation of mean firing rate or firing rate in a specific arm in the ON epoch. The scheme below illustrates step-by-step how to calculate EPM scores during the light ON and OFF epochs from unprocessed data.

Light OFF epoch

location	#spikes	#seconds	Rate (Hz)	Rate (% change from mean)
Up arm (Open arm 1)	40	70	40/70=0.57	$F_U = 100 \times ((0.57-0.87) / 0.87)$ $F_U = -34$
Down arm (Open arm 2)	30	76	0.39	$F_D = -55$
Left arm (closed arm 1)	209	191	1.09	$F_L = +25$
Right arm (closed arm 2)	215	217	0.99	$F_R = +13$
Center	30	46	0.65	$F_C = -25$

Total # of spikes = 40 + 30 + 209 + 215 + 30

Total # of spikes = 524

Total # of seconds = 70 + 76 + 191 + 217 + 46

Total # of seconds = 600

Mean rate = 524 / 600 = 0.87 Hz

EPM score = (A – B) / (A + B), where

A = 0.25 × (| F_L – F_U | + | F_L – F_D | + | F_R – F_U | + | F_R – F_D |) and

B = 0.5 × (| F_L – F_R | + | F_U – F_D |).

A = 64 and B = 16

EPM score (Light OFF)=0.60

Light ON epoch

location	#spikes	#seconds	Rate (Hz)	Rate (% change from mean)
Up arm (Open arm 1)	20	50	20/50=0.4	F_U = 100 × ((0.4-0.62) / 0.62) F_U = -35
Down arm (Open arm 2)	36	80	0.45	F_D = -27
Left arm (closed arm 1)	157	219	0.72	F_L = +15
Right arm (closed arm 2)	112	197	0.56	F_R = -8
Center	48	54	0.88	F_C = 42

Total # of spikes = 373

Total # of seconds = 600

Mean rate=373/600 = 0.62

EPM score = (A – B) / (A + B), where

A = 0.25 × (| F_L – F_U | + | F_L – F_D | + | F_R – F_U | + | F_R – F_D |) and

B = 0.5 × (| F_L – F_R | + | F_U – F_D |).

A = 35 and B = 16

EPM score (Light ON)=0.37

Calculation of EPM scores with simulated data

To calculate if the population of experimentally observed EPM scores was significantly different than expected by chance, a simulated distribution of scores was generated. For each unit with n spikes, 500 simulated scores were generated by calculating the EPM score of n randomly chosen timestamps 500 times. This generated a distribution with 500 × 38 simulated EPM scores. Among these 19000 simulated EPM scores, 12730 (67%) values were negative. The population of positive simulated scores (33%) was almost perfectly evenly divided among close and open-arm preferring cells (3129 and 3141 values, respectively). The significance of the population of experimentally observed EPM scores of all cells was calculated by comparison to the simulated distribution of scores using the Wilcoxon rank-sum test.

Histological verification and confocal microscopy

Mice were deeply anesthetized and transcardially perfused with ice-cold 4% paraformaldehyde (PFA) in PBS (pH 7.4). Brains were fixed overnight in 4% PFA solution and then equilibrated in 30% sucrose in PBS. After the brains were sunken in the sucrose solution, 40 µm-thick coronal slices were cut on a freezing microtome. Placement of the guide cannula, fiberoptics and stereotrode arrays were easily visible after slicing (Supplementary Figs 1-3). Slices were stored in a cryoprotectant solution (a 5:6:9 mixture of glycerol, ethylene glycol and PBS) at 4°C until further processed. Free-floating sections were washed in PBS, incubated for 25 min in 1:50,000 DAPI solution, washed again in PBS and mounted on microscope slides with PVD-DABCO. Confocal images were obtained on a Leica TCS SP5 scanning laser microscope using a 20X/0.70 NA or 40X/1.25 NA oil immersion objective. Images were analyzed using Leica Microsystems LAS AF software.

Calcium imaging and analysis

Coronal brain slices including the BNST were prepared from young mice (n = 4 slices, P8-P10, 300 µm thick) and stained with Oregon Green Bapta-1 AM (OGB) as described

previously[8]. Briefly, slices were cut on a vibratome in ice cold aCSF (in mM: 110 choline chloride, 25 $NaHCO_3$, 10 D-glucose, 7 $MgCl_2$, 3.1 sodium pyruvate, 2.5 KCl, 1.25 NaH_2PO_4, 0.5 $CaCl_2$), and were immediately transferred to recovery aCSF solution (in mM: 125 NaCl, 26 $NaHCO_3$, 10 D-glucose, 3 KCl, 2.5 $MgCl_2$, 1.6 $CaCl_2$, 1.25 NaH_2P0_4) at room temperature for one hour. Then, the slices were moved to an incubation chamber at 32°C containing 2.5 ml recovery ACSF. 10 µl of OGB solution (50 µg OGB dissolved in 9 µl DMSO and 1 µl 20% pluronic acid in DMSO) was directly applied to the slices. After 20-25 min incubation in OGB solution, the slices were moved to experimental aCSF (in mM: 125 NaCl, 26 $NaHCO_3$, 10 D-glucose, 3 KCl, 1.5 $MgCl_2$, 1.6 $CaCl_2$, 1.25 NaH_2P0_4) at room temperature. After one hour, the imaging session began. Images were acquired using an epifluorescence microscope and a CCD camera (50 ms integration time, ~400 frames per trial at ~4 Hz). On a stimulation trial, a 0.2 ms current pulse was applied to a bipolar electrode positioned in the adBNST slice, and within the field of view of the microscope. For a set of stimulation conditions, the amplitude of the current pulse was varied between trials in either increasing or decreasing order in 10 µA steps between 10 and 50 µA. Then, 100 µM APV was applied to the perfusion bath, and the stimulation experiment was repeated. Then, 10 µM NBQX was applied to the bath (while maintaining the concentration of APV) and the stimulation was repeated again. For analysis of OGB fluorescence movies regions of interest (ROI) were drawn around each cell and around the neuropil using a semi-automated procedure. Pixels within each ROI were averaged for each frame, and a time series was generated for each cell. To correct for photobleaching of the fluorophore a bi-exponential was fit to each cell's baseline time series (before stimulation), assuming decay to the cell's minimum fluorescence value, and the fitted curve was subtracted from the cell's time series. A scaled time series of the neuropil was subtracted from each cell's time series to remove global events (the scaling was determined by the least squares difference between the neuropil's and each cell's time series). The change in fluorescence over baseline was computed for each cell for each trial ($\Delta F/F = (F_i - F)/F$, where F_i is the instantaneous fluorescence and F is the mean fluorescence during the baseline). A z-score was computed for each time series based on the standard deviation and mean of the baseline (-40 to 0 s relative to stimulation). Statistically significant activity in a neuron

was defined as any modulation that occurred at least 5 seconds after electrical stimulation (because the neuropil responses decayed back to the baseline for ~5 seconds) and that exceeded z-score of 3.43 ($p < 0.05$; Bonferroni correction).

Statistics

All statistical analysis was performed using GraphPad Prism (GraphPad Software; La Jolla, CA, USA). For EPM and OFT data, two-way repeated measures ANOVA was used, followed by Bonferroni corrected post-hoc tests. P values in the main text indicate the p values for the interaction between the opsin treatment and the epochs, and asterisks (*) in the figures indicate the p values for the post-hoc test at the given epoch. For two-sample comparisons of a single variable (such as % change of respiratory rate of experimental groups and controls or onset latencies of EPSCs and IPSCs), the non-parametric Wilcoxon rank-sum test was used. All tests were two-tailed and had an alpha level of 0.05. Spearman's correlations were used instead of Pearson's correlation because Spearman's correlation is non-parametric, less sensitive to outliers and capable of detecting any monotonic relationship between two variables. Standard errors of means (s.e.m.) were plotted in graphs to show accuracy of estimation of the mean of the population.

References

1. Tye, K. M. *et al.* Amygdala circuitry mediating reversible and bidirectional control of anxiety. *Nature* **471**, 358–362 (2011).
2. Lammel, S. *et al.* Input-specific control of reward and aversion in the ventral tegmental area. *Nature* **491**, 212–217 (2012).
3. Franklin, K. B. J. & Paxinos, G. *The Mouse Brain in Stereotaxic Coordinates, Third Edition*. (Academic Press: 2007).
4. Kügler, S., Kilic, E. & Bähr, M. Human synapsin 1 gene promoter confers highly neuron-specific long-term transgene expression from an adenoviral vector in the adult rat brain depending on the transduced area. *Gene Ther.* **10**, 337–347 (2003).
5. McDonald, A. J., Muller, J. F. & Mascagni, F. GABAergic innervation of alpha type II calcium/calmodulin-dependent protein kinase immunoreactive pyramidal neurons in the rat basolateral amygdala. *J. Comp. Neurol.* **446**, 199–218 (2002).

6. Dong, H. W., Petrovich, G. D. & Swanson, L. W. Topography of projections from amygdala to bed nuclei of the stria terminalis. *Brain Res. Brain Res. Rev.* **38**, 192–246 (2001).
7. Adhikari, A., Topiwala, M. A. & Gordon, J. A. Single units in the medial prefrontal cortex with anxiety-related firing patterns are preferentially influenced by ventral hippocampal activity. *Neuron* **71**, 898–910 (2011).
8. Dawitz, J., Kroon, T., Hjorth, J. J. J. & Meredith, R. M. Functional calcium imaging in developing cortical networks. *J Vis Exp* (2011).doi:10.3791/3550

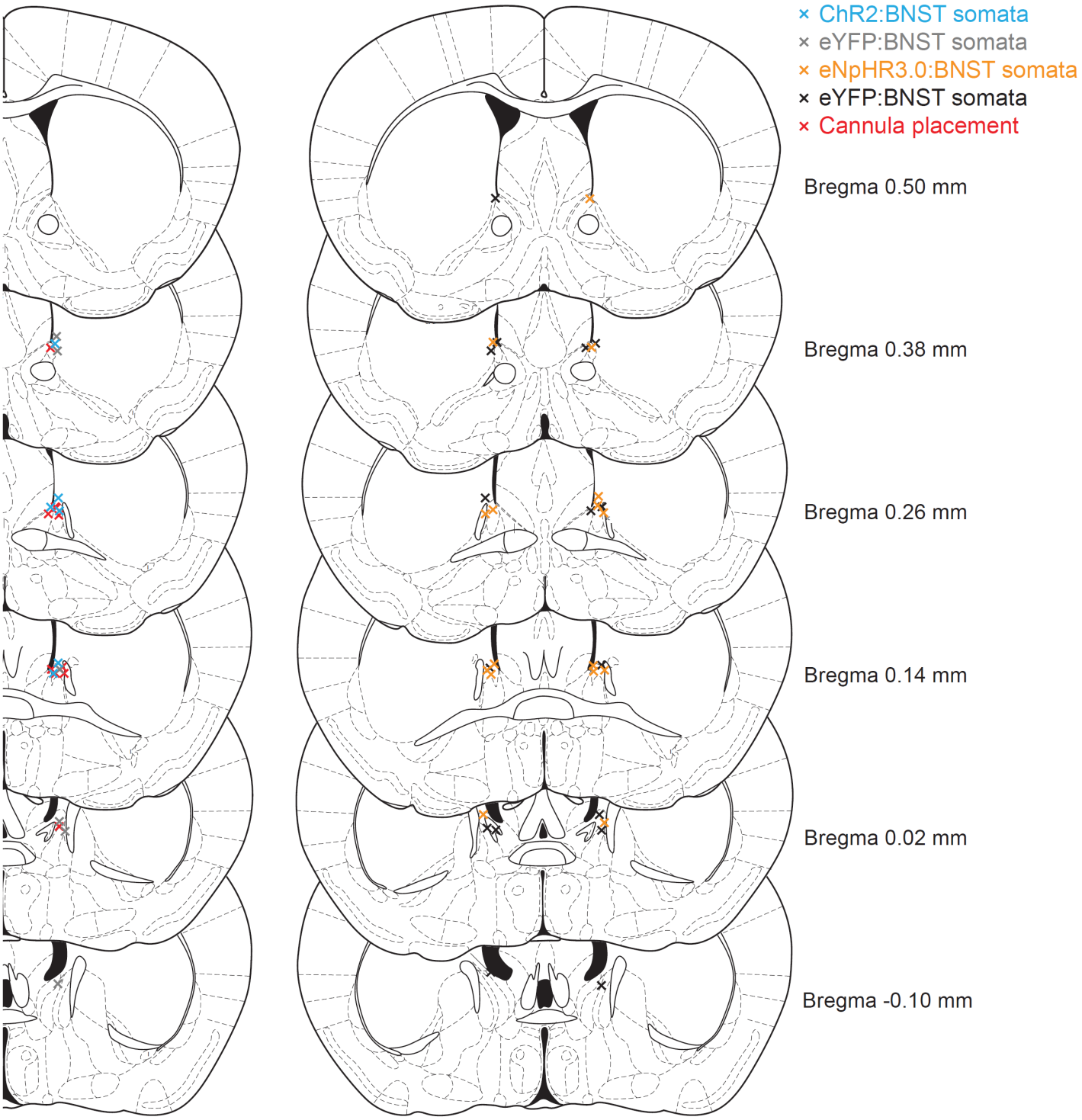

Supplementary Figure 1. Placement of fiberoptics and cannula guides targeting the BNST.

(Left) Unilateral placement of fiberoptic tips for ChR2:BNST somata mice and eYFP controls are indicated (cyan and gray, respectively). Guide cannula tip locations are indicated in red. All unilateral surgeries were counter-balanced for hemisphere. **(Right)** Bilateral placements of the fiberoptic tips for eNpHR3.0:BNST somata mice and controls are indicated (orange and black, respectively). Numbers indicate antero-posterior coordinates from bregma.

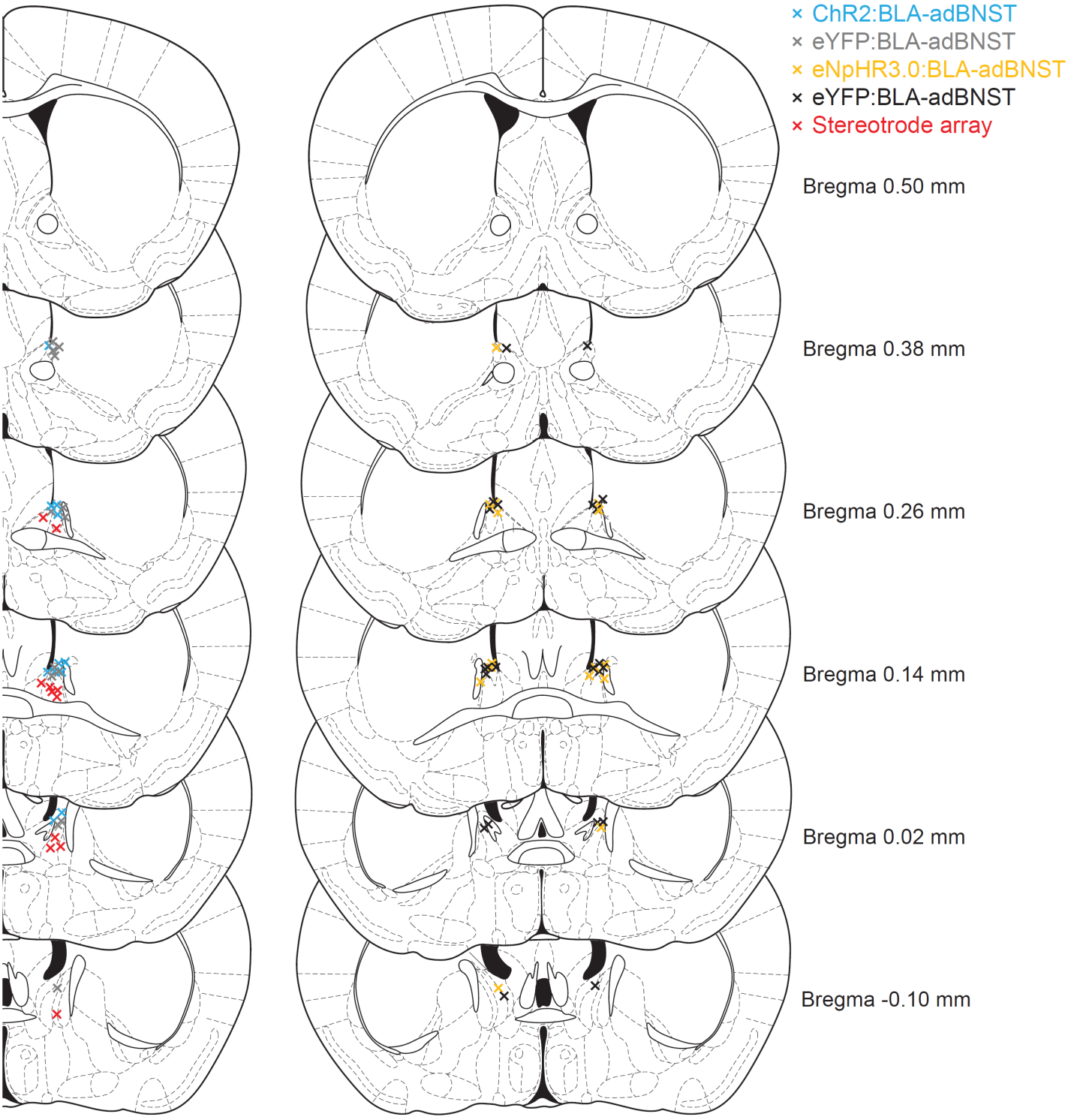

Supplementary Figure 2. Placement of fiberoptics and stereotrode arrays targeting the adBNST.

(Left) Unilateral placements of fiberoptic tips for ChR2:BLA-adBNST mice and eYFP controls are indicated (cyan and gray, respectively). Tips of stereotrode arrays for *in vivo* recording are indicated in red. All unilateral surgeries were counter-balanced for hemisphere. **(Right)** Bilateral placements of the fiberoptic tips for eNpHR3.0:BLA-adBNST mice and controls are indicated (yellow and black, respectively). Numbers indicate antero-posterior coordinates from bregma.

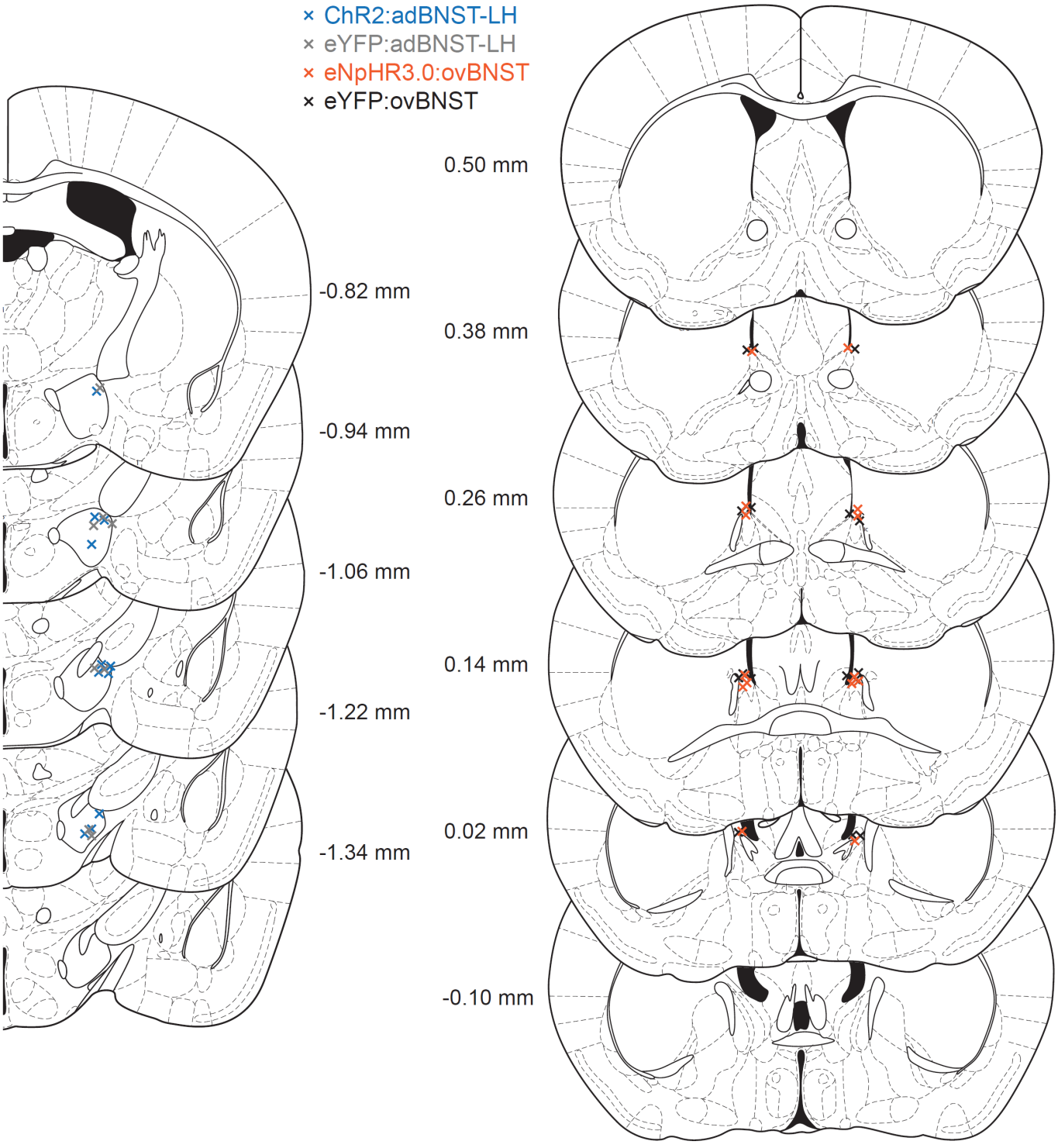

Supplementary Figure 3. Placement of fiberoptics targeting the ovBNST and the LH.

(Left) Unilateral placements of the tip of the fiberoptics for ChR2:adBNST-LH mice and eYFP controls are indicated (blue and gray, respectively). All unilateral surgeries were counter-balanced for hemisphere. **(Right)** Bilateral placements of fiberoptic tips for eNpHR3.0:ovBNST mice and controls are indicated (yellow and black symbols, respectively). Numbers indicate antero-posterior coordinates from bregma.

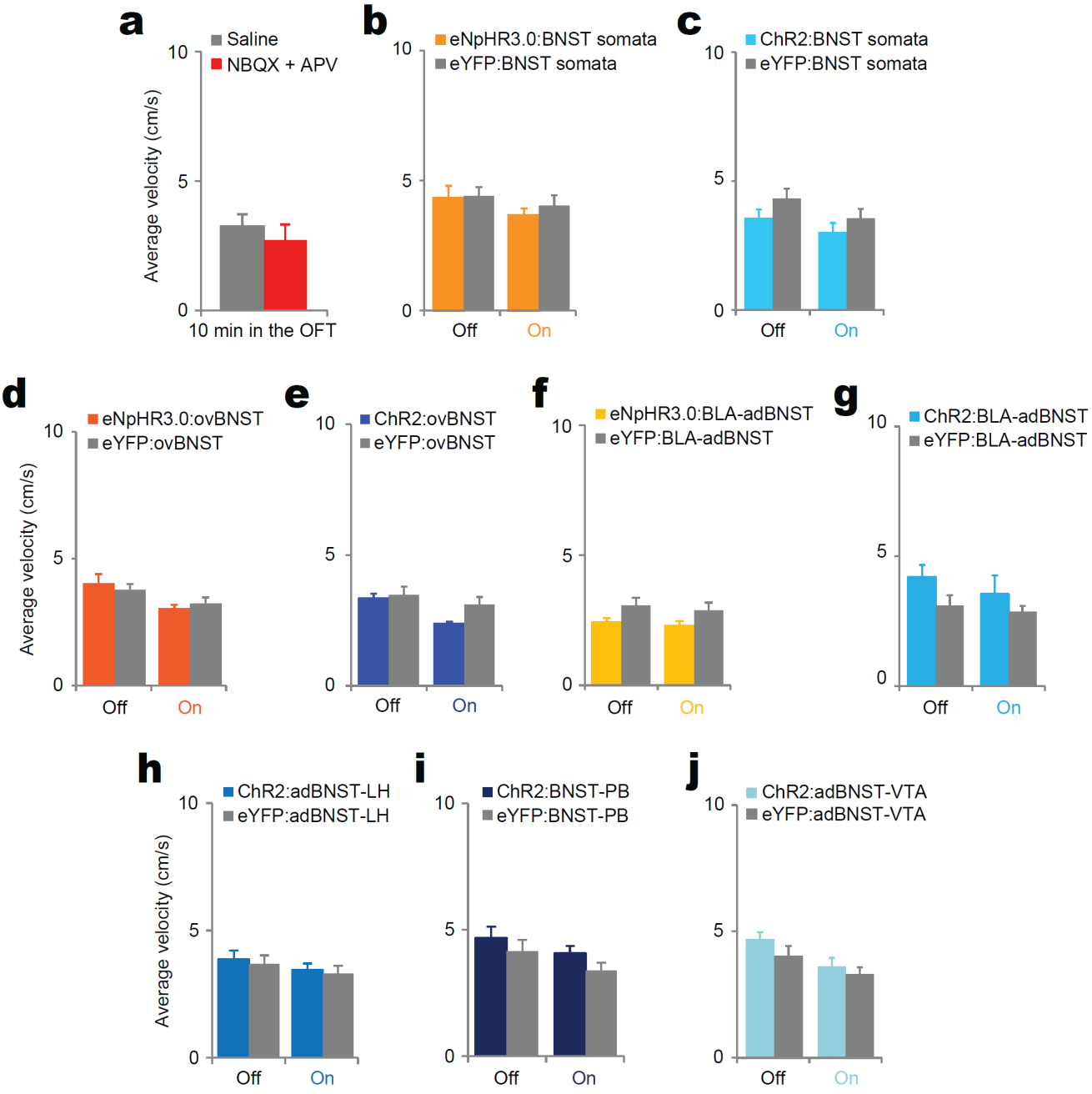

Supplementary Figure 4. Locomotor activity was not altered by any of the manipulations performed.

(a) Locally infusing NBQX and APV into the BNST (*n* = 5 for exp, *n* = 5 for controls; p > 0.05), **(b)** inhibiting BNST somata (*n* = 10 for exp; *n* = 11 for controls; p > 0.05), **(c)** stimulating BNST somata (*n* = 6 for exp; *n* = 6 for controls; p > 0.05), **(d)** inhibiting the ovBNST (*n* = 8 for exp; *n* = 8 for controls; p > 0.05), **(e)** stimulating ovBNST (*n* = 7 for exp; *n* = 7 for controls; p > 0.05), **(f)** inhibiting BLA fibers in the adBNST (*n* = 11 for exp; *n* = 11 for controls; p > 0.05), **(g)** stimulating BLA fibers in the adBNST (*n* = 8 for exp; *n* = 8 for controls; p > 0.05), **(h)** stimulating adBNST fibers in the LH (*n* = 11 for exp; *n* = 8 for controls; p > 0.05), **(i)** stimulating BNST fibers in the PB (*n* = 8 for exp; *n* = 7 for controls; p > 0.05) or **(j)** stimulating adBNST fibers in the VTA (*n* = 8 for exp; *n* = 7 for controls; p > 0.05) had no detectable effect on mean locomotion speed. Values are mean ± s.e.m.

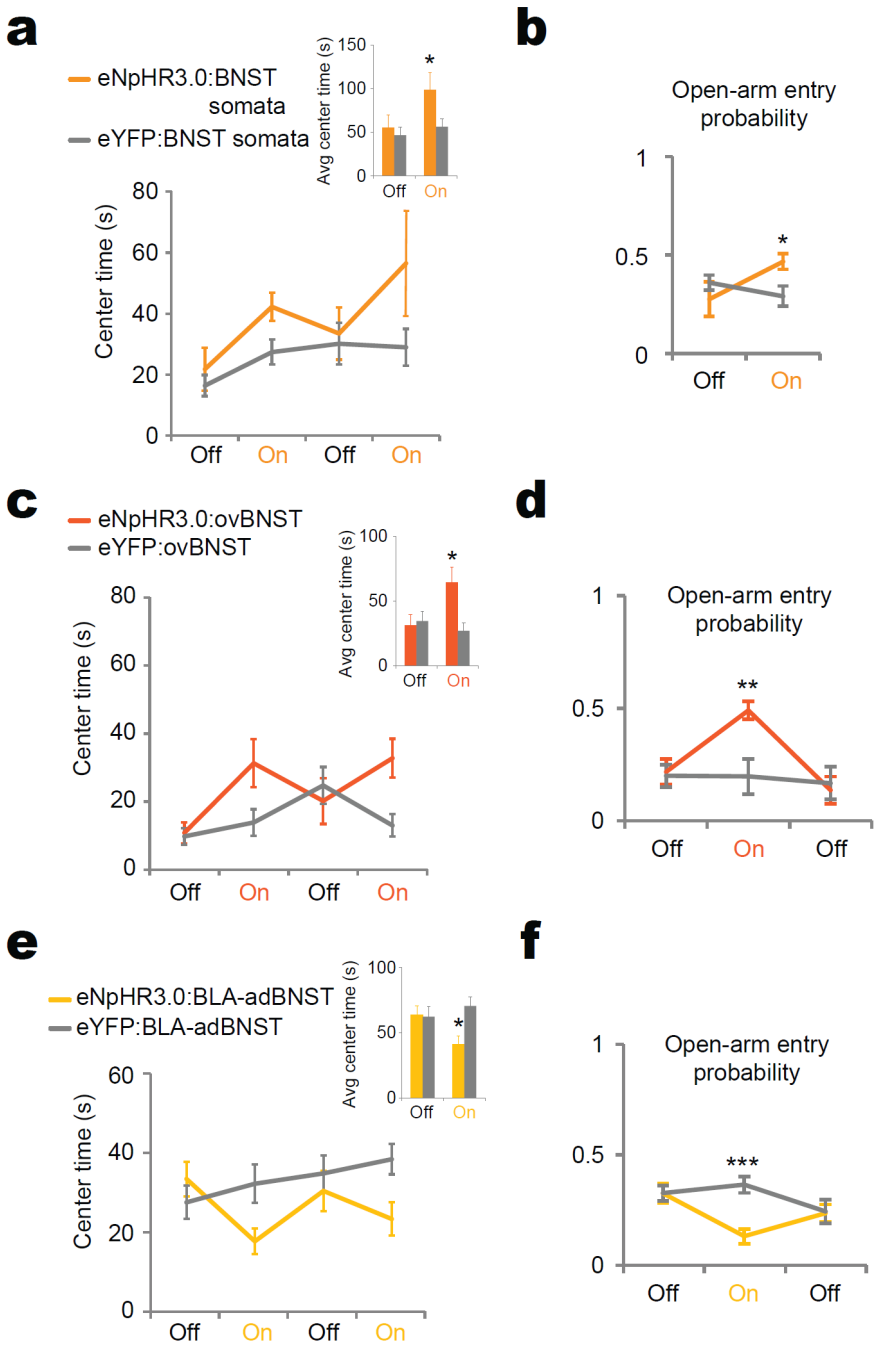

Supplementary Figure 5. Functional heterogeneity in the BNST in anxiety paradigms.

Yellow light in eNpHR3.0:BNST somata mice increased center time in the OFT **(a)** and open-arm entry probability in the EPM **(b).** Yellow light in eNpHR3.0:ovBNST mice increased center time in the OFT **(c)** and open-arm entry probability in the EPM **(d)**. Yellow light in eNpHR3.0:BLA-adBNST mice reduced center time in the OFT **(e)** and open-arm entry probability in the EPM **(f)**. Values are mean ± s.e.m. *, ** and *** indicate $p<0.05$, 0.01 and 0.001, respectively. Statistical analysis in Supplementary Information. Data in this figure represent additional behavioral results from the same cohorts shown in **Fig. 1**.

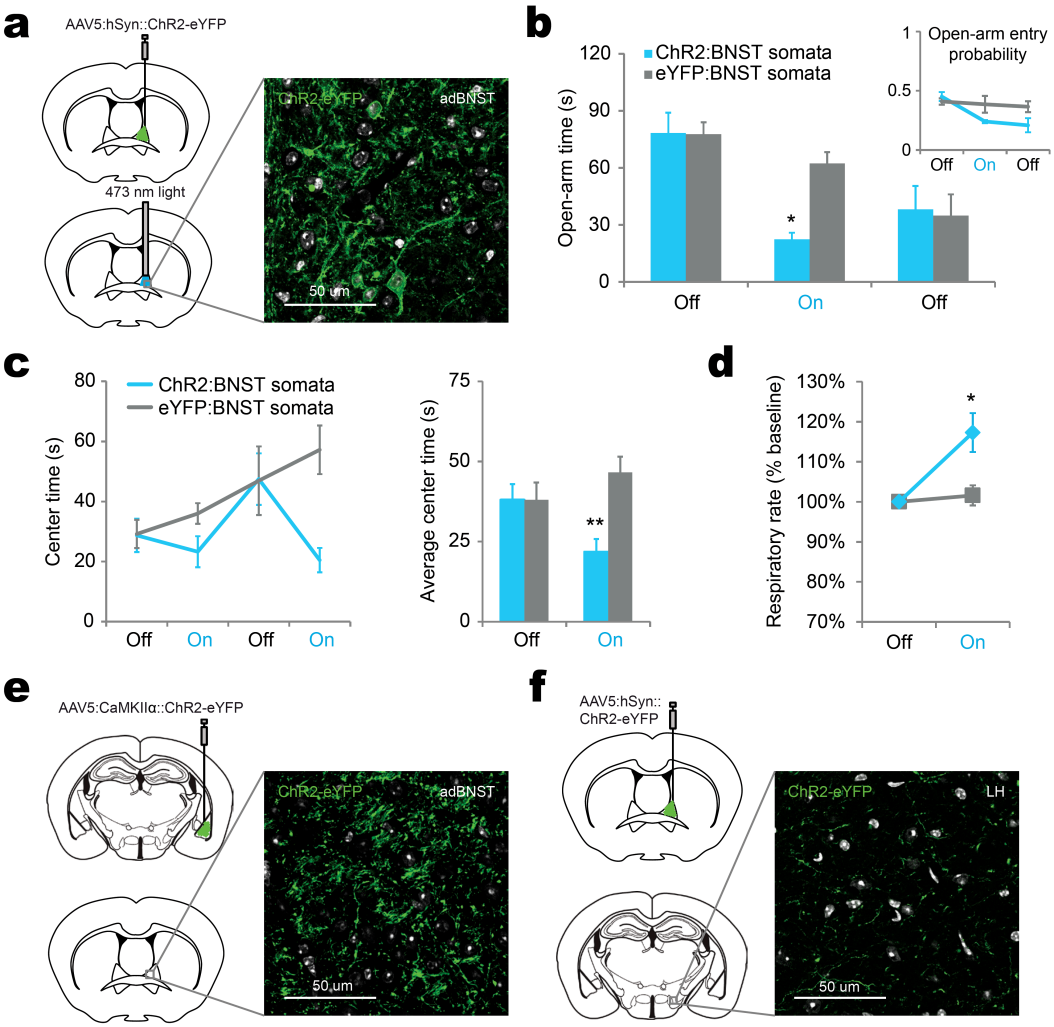

Supplementary Figure 6. Optogenetic stimulation of BNST somata increases anxiety-related behavior.

(a) 6-8 week old mice received a unilateral injection of 0.5 µl AAV5:hSyn::ChR2-eYFP (ChR2:BNST somata; *n* = 6) or AAV5:hSyn::eYFP (eYFP:BNST somata; *n* = 6) in the BNST and were implanted with fiberoptics directly above the BNST. Behavioral assays were performed 4 weeks after injection. Confocal image shows expression of ChR2-eYFP in BNST cell bodies (40X objective, 3X optical zoom, single plane). **(b)** Mice were run on the elevated plus maze for a 15-min session, consisting of 5-min light OFF/ON/OFF epochs. Blue light stimulation delivery during the ON epoch (5 ms pulse width, 10 Hz) in the ChR2:BNST somata group decreased open-arm time and open-arm entry probability (inset) relative to eYFP controls ($F_{2,18}$ = 5.04, $p < 0.05$; inset: $F_{2,18}$ = 3.94, $p < 0.05$). **(c)** A week later, mice were run on the open field for a 20-min session, consisting of 5-min light OFF/ON/OFF/ON epochs. Blue light stimulation decreased center time in the OFT during light on epochs compared to eYFP controls (left, $F_{3,30}$ = 3.89, $p < 0.05$; right, $F_{1,10}$ = 16.02, $p < 0.01$). **(d)** A week later, respiratory rate was measured from the same mice for 6 min, and light stimulation was given for the last 3 minutes. Light stimulation increased respiratory rate ($p < 0.05$, Wilcoxon signed-rank test). **(e-f)** For comparison with **(a)**, high-resolution images of BLA fibers expressing ChR2-eYFP in the adBNST **(e)** and adBNST fibers expressing ChR2-eYFP in the LH **(f)** are shown. For statistical analysis, two-way repeated measures ANOVA was used unless otherwise indicated. Values are mean ± s.e.m. * and ** indicate p<0.05 and <0.01, respectively.

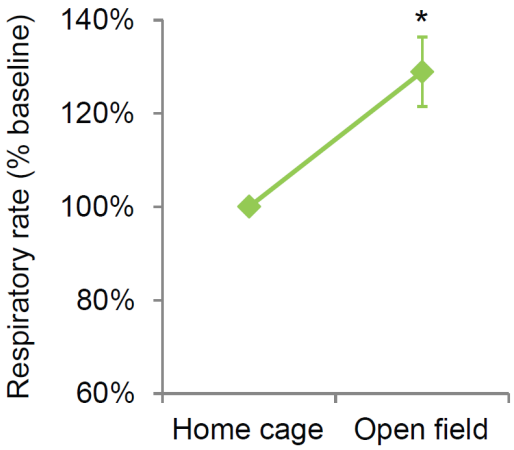

Supplementary Figure 7. Respiratory rate increases in an anxiogenic environment.

12-16 week old naive mice (*n* = 7) were handled for 3 days and acclimated to the collar clip used for the respiratory rate measurement. Respiratory rate was first recorded in the home cage or the open field for 3 min. Mice were given 5 min of resting in a new clean cage and then recorded in the other environment for 3 min. The order of recordings was counterbalanced across animals. Note that respiratory rate was significantly increased by placing the animals into an open field apparatus, an anxiogenic environment, compared to the values measured in the home cage ($p < 0.05$, Wilcoxon signed-rank test). *, $p<0.05$.

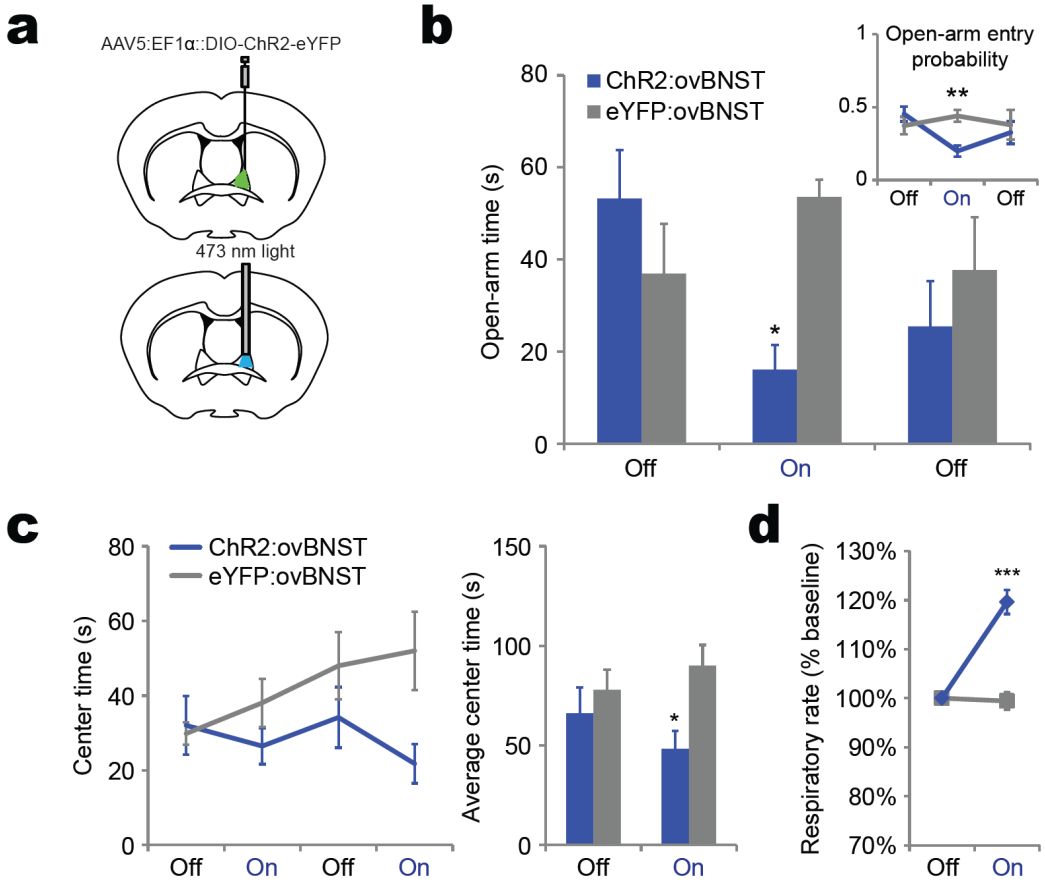

Supplementary Figure 8. Optogenetic stimulation of the ovBNST increases anxiety-related behavior.

(a) 6-8 week old Drd1a-Cre mice received unilateral injection of 0.5 µl AAV5:EF1α::DIO-ChR2-eYFP (ChR2:ovBNST; *n* = 7) or AAV5:EF1α::DIO-eYFP (eYFP:ovBNST; *n* = 7) in the ovBNST and were implanted with fiberoptics directly above the ovBNST. Behavioral assays were performed 4 weeks after injection. **(b)** Mice were run on the elevated plus maze for a 15-min session, consisting of three 5-min light OFF/ON/OFF epochs. Blue light stimulation delivery during the ON epoch (5 ms pulse width, 10 Hz) in the ChR2:BNST somata group decreased open-arm time and open-arm entry probability (inset) relative to eYFP controls ($F_{2,24}$ = 6.208, $p < 0.05$; inset: $F_{2,24}$ = 4.078, $p < 0.05$). **(c)** A week later, mice were run on the open field for a 20-min session, consisting of 5-min light OFF/ON/OFF/ON epochs. Blue light stimulation decreased center time in the OFT during light on epochs compared to eYFP controls (left, $F_{3,36}$ = 2.311, $p = 0.0927$; right, $F_{1,12}$ = 6.206, $p < 0.05$). **(d)** A week later, respiratory rate was measured from the same mice for 6 min, and light stimulation was given for the last 3 minutes. Light stimulation increased respiratory rate ($p < 0.001$, Wilcoxon signed-rank test). Values are mean ± s.e.m. *, ** and *** indicate p<0.05, 0.01 and 0.001, respectively.

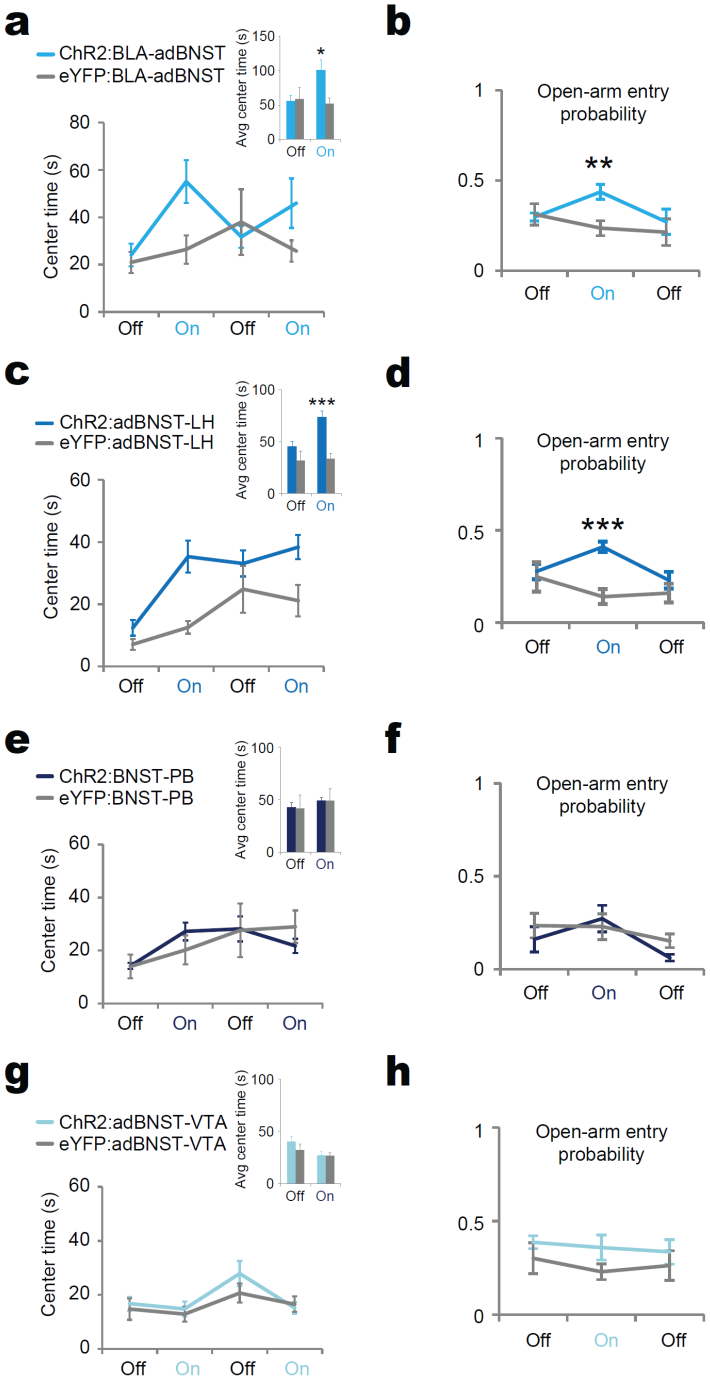

Supplementary Figure 9. Stimulation of adBNST projection to the LH, but not to the PB or VTA, is anxiolytic.

Blue light in ChR2:BLA-adBNST mice increased center time in the OFT **(a)** and open-arm entry probability in the EPM **(b).** Blue light in ChR2:adBNST-LH mice increased center time in the OFT **(c)** and open-arm entry probability in the EPM **(d)**. Blue light in ChR2:BNST-PB mice had no effect in center time in the OFT **(e)** and open-arm entry probability in the EPM **(f)**. Blue light in ChR2:adBNST-VTA mice had no effect in center time in the OFT **(g)** and open-arm entry probability in the EPM **(h)**. Values are mean ± s.e.m. *, ** and ***, indicate p<0.05, 0.01 and 0.001, respectively. Statistical analysis in Supplementary Information. Data in this figure are additional behavioral results from the same cohorts shown in **Fig. 2**.

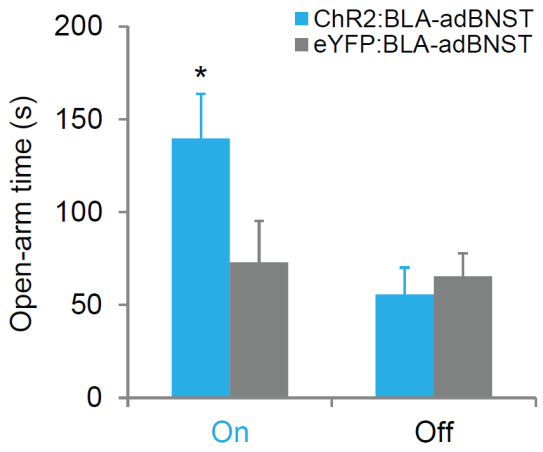

Supplementary Figure 10. Optogenetic stimulation of the BLA-adBNST projection reduces anxiety-related behavior in the EPM in the first 5 minutes of EPM exposure.

To demonstrate that optogenetic stimulation of the BLA-adBNST projection reduces anxiety-like behavior in the more commonly used 5-minute elevated plus maze test, a separate cohort of group-housed ChR2:BLA-adBNST mice was generated. 6-8 week old mice received a unilateral injection of 0.5 µl AAV5:CaMKIIα::ChR2-eYFP (ChR2:BLA-adBNST; *n* = 8) or AAV5: CaMKIIα::eYFP (eYFP:BLA-adBNST; *n* = 6) in the BLA and were implanted with fiberoptics directly above the BNST. Behavioral assays were performed 8 weeks after injection. Mice were run on the elevated plus maze for a 10-min session, consisting of 5-min light ON/OFF epochs. Blue light stimulation delivery during the ON epoch (5 ms pulse width, 10 Hz) in the ChR2:BLA-adBNST group decreased open-arm time relative to eYFP controls (two-way repeated measures ANOVA, $F_{1,12} = 8.347$, $p < 0.05$; post-hoc Bonferroni *t*-test, $p < 0.05$ at light ON epoch). Note the presence of an anxiolytic effect in the first 5 minutes (ON epoch). Values are mean ± s.e.m.

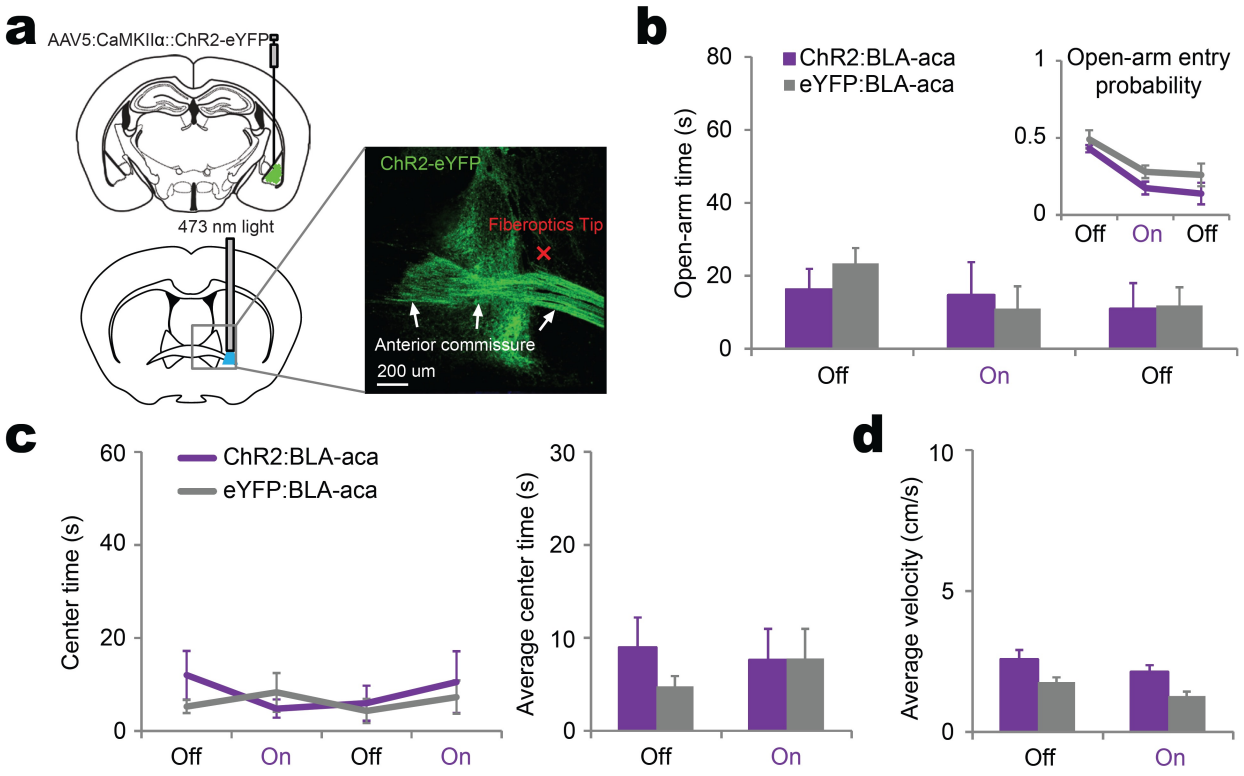

Supplementary Figure 11. Stimulating BLA fibers in the anterior commissure (aca) does not affect anxiety-related behavior.

(a) 6-8 week old mice received an unilateral injection of 0.5 µl AAV5:CaMKIIα::hChR2(H134R)-eYFP (ChR2:BLA-aca; *n* = 5) or AAV5:CaMKIIα::eYFP (eYFP:BLA-aca; *n* = 5) in the BLA and were implanted with fiberoptics directly above the BNST. Behavioral experiments were conducted 8 weeks after the injection. Confocal image shows robust expression of ChR2-eYFP in BLA fibers passing through the anterior commissure. Blue light stimulation (5 ms pulse width, 10 Hz) in the ChR2:BLA-aca group (*n* = 5) did not affect open-arm time and probability of open-arm entry in the elevated plus maze test (15-min session divided into 5-min OFF/ON/OFF epochs) **(b),** center time **(c)** and locomotor activity in the open field test (20-min session consisting of 5-min OFF/ON/OFF/ON epochs) **(d)** during light-ON epochs. All p > 0.05, two-way repeated measures ANOVA. Values are mean ± s.e.m.

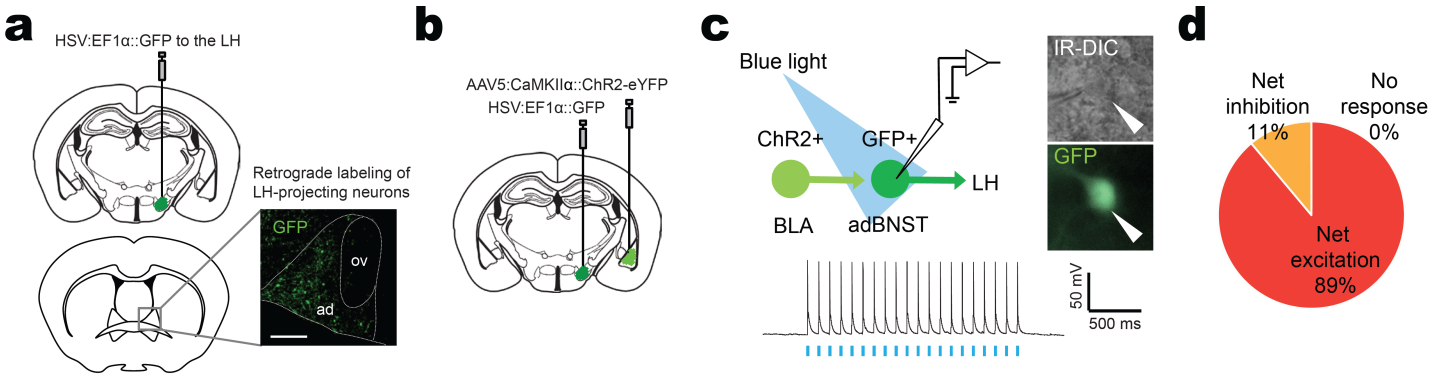

Supplementary Figure 12. adBNST neurons projecting to the LH are innervated by BLA axon terminals.

(a) Three 6 week old mice were injected in the LH with 0.5 µl of herpes simplex virus (HSV), a retrogradely propagating virus, encoding GFP under the EF1α promoter (HSV:EF1α::GFP). 5 days after the injection, mice were perfused and 40 µm coronal sections containing the BNST were prepared for confocal microscopy. GFP-positive retrogradely-labeled neurons were observed only in the adBNST, but not in the ovBNST, in all mice. Representative confocal image shows z-max projection of a 12 µm section. Scale bar, 200 µm. **(b)** Three 6 week old mice were injected with 0.5 µl HSV:EF1α::GFP in the LH and with 0.5 µl AAV5:CaMKIIα::ChR2-eYFP in the BLA. 3-5 days after the injection, acute slices containing the BNST were prepared for slice patch-clamp recording. **(c)** GFP-expressing neurons in the adBNST were recorded during optical stimulation of BLA terminals in the BNST. Representative current-clamp trace from a GFP(+) adBNST neuron (V_m=~-60 mV) is shown at the bottom. **(d)** Most neurons were excited at resting potential in current clamp mode (8/9 neurons). Remarkably, every labeled neuron showed light-evoked responses (*n* = 9 adBNST neurons).

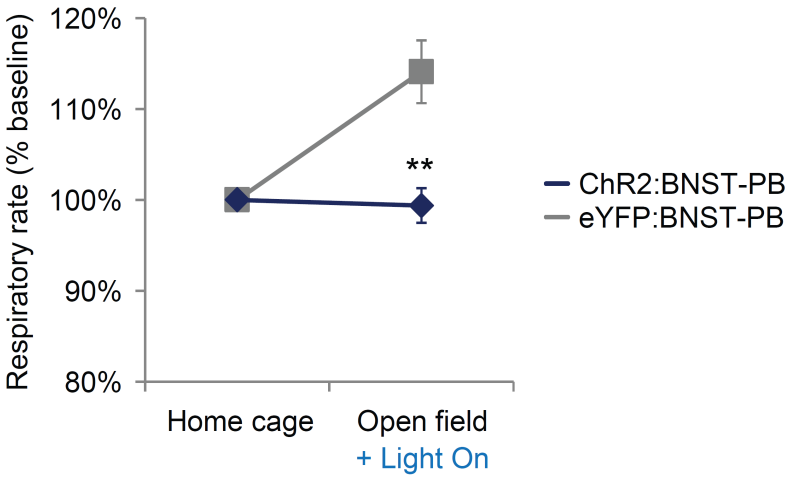

Supplementary Figure 13. Respiratory rate increase in an anxiogenic environment is attenuated by stimulating the BNST-PB projection.

10 week old mice received unilateral injection of 0.5 µl AAV5:hSyn::ChR2-eYFP (ChR2:BNST-PB; *n* = 7) or AAV5:hSyn::eYFP (eYFP:BNST-PB; *n* = 5) in the BNST and were implanted with fiberoptics directly above the PB. The experiment began 16 weeks after the injection. Mice were handled for 3 days and acclimated to the collar clip for the respiratory rate measurement. Respiratory rate was first recorded in the home cage or the open field for 3 min. Mice were allowed to rest in a new clean cage for 5 min, and were then recorded in the other environment for 3 min. Blue laser stimulation was delivered (5 ms pulse width, 10 Hz) in the open field. The order of recording environments was counterbalanced across animals. Respiratory rate was significantly increased by placing the animals into an open field paired with light stimulation in eYFP:BNST-PB mice compared to the values measured in the home cage. This increase was significantly attenuated in ChR2:BNST-PB mice ($p<0.01$, Wilcoxon rank-sum test), indicating that stimulating the BNST-PB projection is sufficient to reduce an anxiogenic stimulus-elicited increase in respiratory rate.

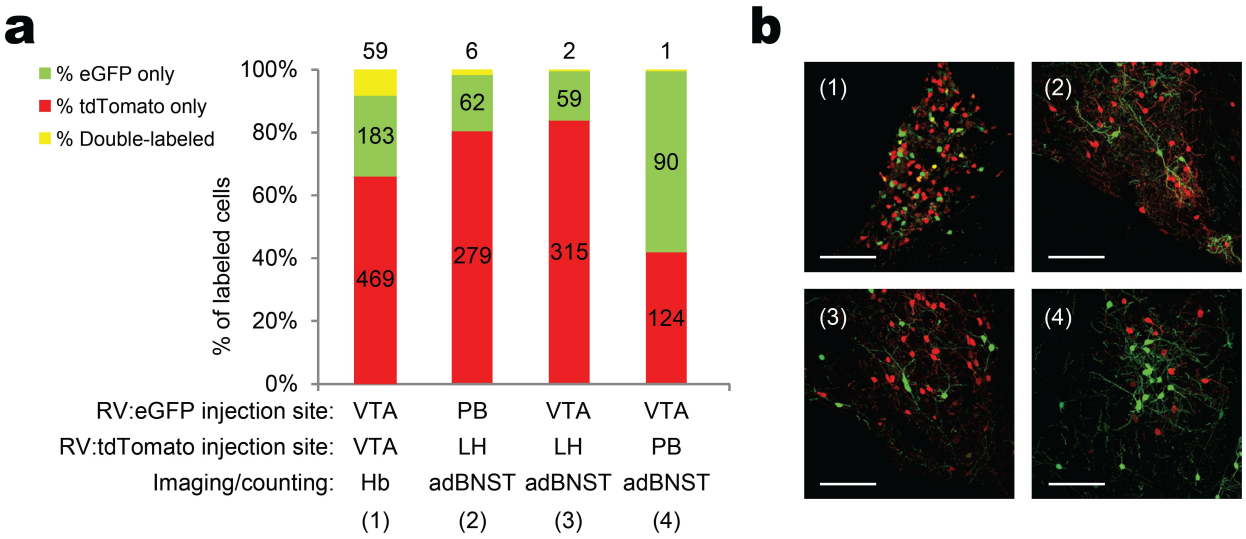

Supplementary Figure 14. Subpopulations of adBNST neurons project to the LH, PB and VTA.

(a-b) To examine the degree of overlap between subpopulations of BNST neurons that project to LH, PB and VTA, 0.5 µl of rabies virus encoding eGFP (RV:eGFP) and tdTomato (RV:tdTomato) were injected in the indicated regions of 6 week old mice. Four days after the injection, mice were perfused and 40 µm coronal sections were prepared for confocal microscopy. **(a)** Summary plot of % labeled adBNST neurons. Injecting a mixture of RV-eGFP and RV-tdTomato viruses in the VTA yielded 8.3% double-labeled neurons in the habenula (Hb). However, injecting RV:eGFP and RV:tdTomato into any two of LH, PB or VTA co-labeled very few BNST neurons (1.7% for PB/LH, 0.5% for VTA/LH, 0.0% for VTA/PB). All groups displayed a significantly smaller fraction of co-labeled cells than the positive control VTA-VTA group ($p<0.0001$), suggesting that subpopulations of adBNST neurons projecting to the LH, PB and VTA are not completely overlapping. Numbers indicate cell counts. **(b)** Representative images showing fluorophore expression in the indicated regions (green: eGFP, red, tdTomato, yellow: double-labeled). (1), single plane; (2-4) z-max projections of 20-µm sections. Scale bar, 100 µm. Note that another positive control showing that neurons can get infected twice by these same rabies virus preparations can be found in Lammel *et al*. *Nature*, 2012 Nov 8;491(7423):212-7 (2012). Statistical analysis in Supplementary Information.

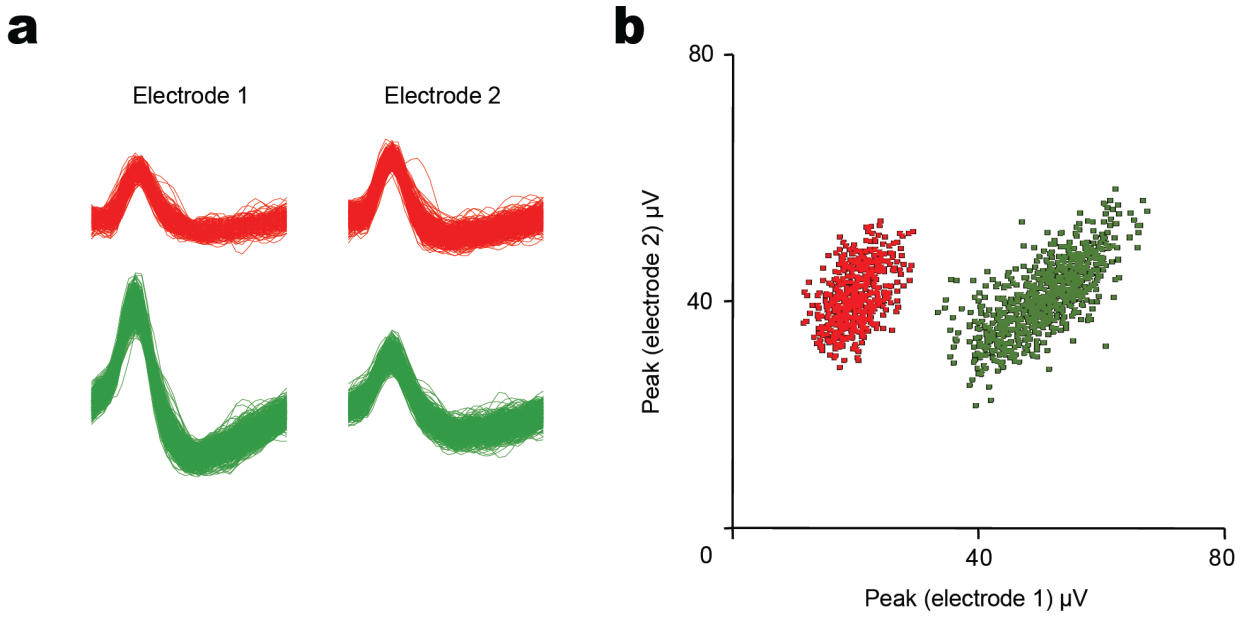

Supplementary Figure 15. Isolation of single units via stereotrodes.

Mice were implanted with microdrives containing 8 tungsten stereotrodes. **(a)** Examples of spikes from two adBNST single units simultaneously recorded by the same stereotrode. **(b)** Scatterplot of peak on electrode 1 against peak on electrode 2. The spikes from these two single units form well-isolated clusters. Spikes were sorted offline using SpikeSort3D software (Neuralynx).

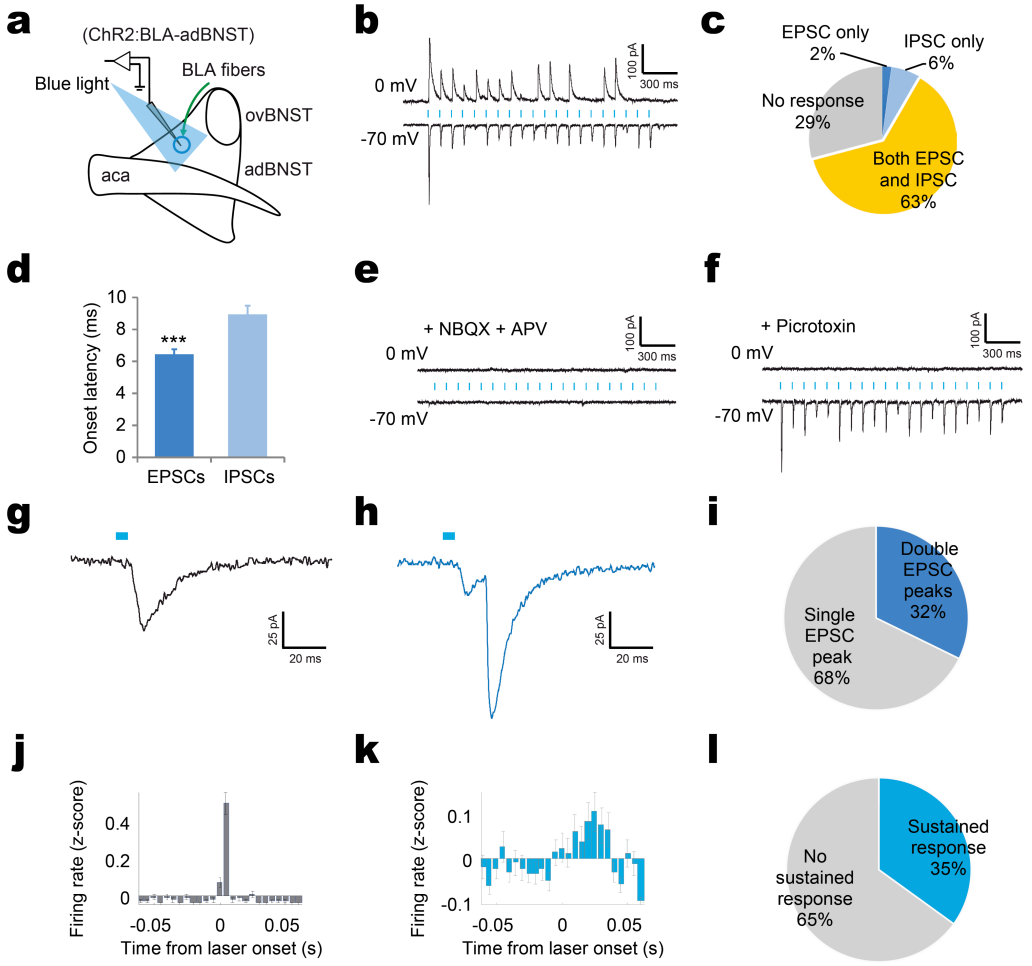

Supplementary Figure 16. Evidence for feed-forward inhibitory and excitatory circuitry in the adBNST.

To examine the connectivity between the BLA and BNST, **(a)** eight 4-week old mice were injected with 0.5 µl AAV5:CaMKIIα::ChR2-eYFP in the BLA. 4 weeks after injection, acute slices containing the BNST and BLA axon fibers were prepared for slice patch-clamp recording. See **Fig. 3** for related current-clamp and *in vivo* recording experiments. **(b)** Representative voltage-clamp traces from an adBNST neuron held at 0 mV (top) and -70 mV (bottom), displaying IPSCs and EPSCs in response to 10 Hz, 5-ms blue light pulses. **(c)** Most light-responsive neurons exhibited both EPSCs and IPSCs (*n* = 48 adBNST neurons). These IPSCs are likely not monosynaptic, but indirectly driven by local adBNST neurons, since: 1) we optogenetically stimulated an excitatory projection, 2) EPSCs had shorter latencies than IPSCs ($p<0.001$; see (d) below), and 3) bath application of the excitatory-glutamate receptor antagonists NBQX (2,3-dihydroxy-6-nitro-7-sulfamoyl-benzo[f]quinoxaline-2,3-dione) and APV ((2R)-amino-5-phosphonopentanoate) blocked both EPSCs and IPSCs, whereas bath application of the $GABA_A$ receptor antagonist picrotoxin blocked only IPSCs (see (e,f) below). **(d)** Onset latency of EPSCs was shorter than that of IPSCs (*n* = 14 for EPSCs, *n* = 16 for IPSCs. $p < 0.001$, Wilcoxon rank-sum test). **(e)** Bath application of 10 µM NBQX and 50 µM APV abolished both IPSCs and EPSCs (*n* = 4) (top), whereas **(f)** 100 µM picrotoxin blocked IPSCs but not EPSCs (*n* = 4) (bottom). Representative voltage-clamp traces from adBNST neurons held at -70 mV, displaying single peak **(g)** or double peaks **(h)** in response to a 5-ms blue light pulse. **(i)** Summary of responses observed in the adBNST neurons that exhibited EPSCs (*n* = 31). Four 6 week old mice were

injected with 0.5 µl AAV5:CaMKIIα::ChR2-eYFP in the BLA and implanted with a drivable microdrive containing 8 stereotrodes and a fiberoptic in adBNST to allow simultaneous optogenetic stimulation and recording of adBNST neurons. Representative PSTHs of adBNST single unit recordings showing increased activity time-locked to a 5-ms laser pulse **(j)** or persistent activity even after the end of the laser pulse **(k)**. **(l)** Summary of adBNST single units that exhibited excitatory responses to blue light (*n* = 20). Together with the results from Figure 3, these data demonstrate that the adBNST neurons receive both direct excitatory inputs and indirect inhibitory inputs from the BLA, but the most common net response is excitation.

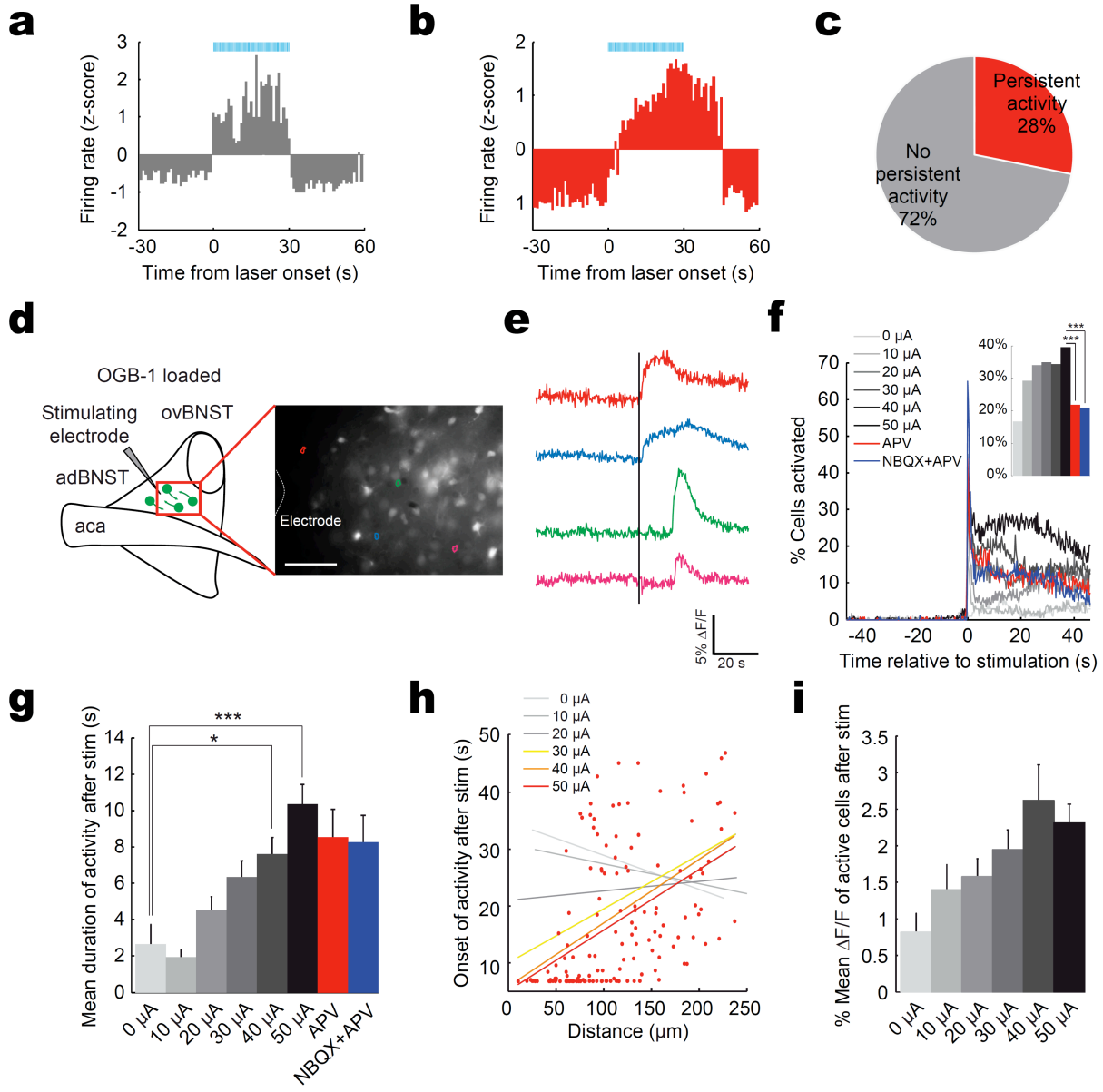

Supplementary Figure 17. Recurrent excitation may enable coordinated recruitment of BNST downstream projections.

(a-c) Same experiment as **Fig. 3a-c**. ChR2:BLA-adBNST mice implanted with fiberoptic-stereotrode array in the adBNST received a 10-Hz light pulse train (5 ms pulse width) for 30-s period (bottom). Recruitment of different populations of adBNST projection neurons could involve recurrent excitation in the adBNST, consistent with findings from these *in vivo* multiunit recordings; persistent activity was seen in 28% of recordings after the end of BLA fiber stimulation. Shown are representative PSTHs of adBNST multiunit recordings showing increased activity time-locked to a laser pulse train. The example in **(b)** but not in **(a)**, exhibits persistent activity even after the end of laser stimulation. **(c)** Summary of adBNST multiunit recordings (n = 103). **(d)** To test for persistent activity in a reduced BNST slice, we performed Ca^{2+} imaging, and found persistent activity in the adBNST slice following a single brief 0.2 ms stimulus. Oregon Green BAPTA-1 (OGB-1)-loaded adBNST neurons (image) were monitored in response to varying current levels of electrical stimulation. **(e)** Representative trace of cells showing persistent activity induced by 0.2-ms electrical stimulation, including late onset activation for neurons over 100 µm from the electrode. Location of each color-coded cell is indicated in **(d)**. Vertical line

indicates the time of electrical stimulation. **(f)** The fraction of activated cells increased with ascending electrical stimulation amplitude, and was reduced by over 40% after bath application of either 100 μM APV alone or 10 μM NBQX and 100 μM APV. (Histogram bin size: 234 ms = 1 frame). **(g)** Duration of activation of neurons was enhanced by increasing amplitude of electrical stimulation indicating recruitment of persistent activity. Interestingly, while the fraction of activated neurons was reduced after application of NBQX and APV, the duration of activation for activated neurons was similar to the control condition (50 μA), suggesting that the reduction of excitatory transmission in the APV and NBQX conditions did not completely block persistent activity. **(h)** Scatterplot of onset of activity evoked by the 50 μA stimulus against the distance of the cell from the electrode tip. Regressed lines for different stimulation intensity are shown, indicating a propagation of onset of activity over distance ($p<0.001$ for 30, 40 and 50 μA stimulus conditions). **(i)** Mean $\Delta F/F$ of activated cells following electrical stimulation. Activity of cells averaged over the post-stimulation period ($\%\Delta F/F$) that were activated by electrical stimulation shows an increasing trend as the stimulation intensity is increased. Values are mean ± s.e.m. * and *** indicate $p<0.05$ and 0.001, respectively. Statistical analysis in Supplementary Information.

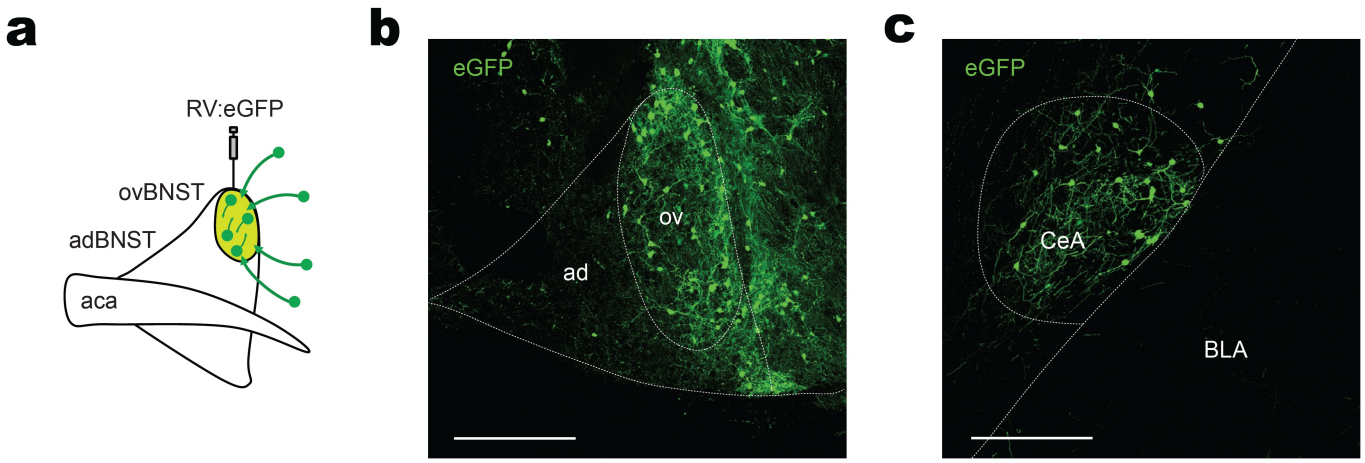

Supplementary Figure 18. The adBNST weakly projects to the ovBNST.

(a) To examine connectivity between the ovBNST and the adBNST, rabies virus in which the glycoprotein is replaced by enhanced green fluorescent protein (RV-eGFP) was injected to the ovBNST. **(b)** Representative fluorescence image showing eGFP expression in local ovBNST neurons. Note the scarcity of eGFP-expressing neurons in the adBNST, indicating weak projections from the adBNST to the ovBNST. **(c)** Fluorescence image showing restricted eGFP expression in the CeA in the amygdala. Since the CeA projects to both the ovBNST and the adBNST while the BLA projects only to the adBNST but not to the ovBNST, this result indicates that the RV-eGFP injection in the ovBNST did not spread to the adBNST. All scale bars are 200 μm. All images are z-max projection of 20-μm section.

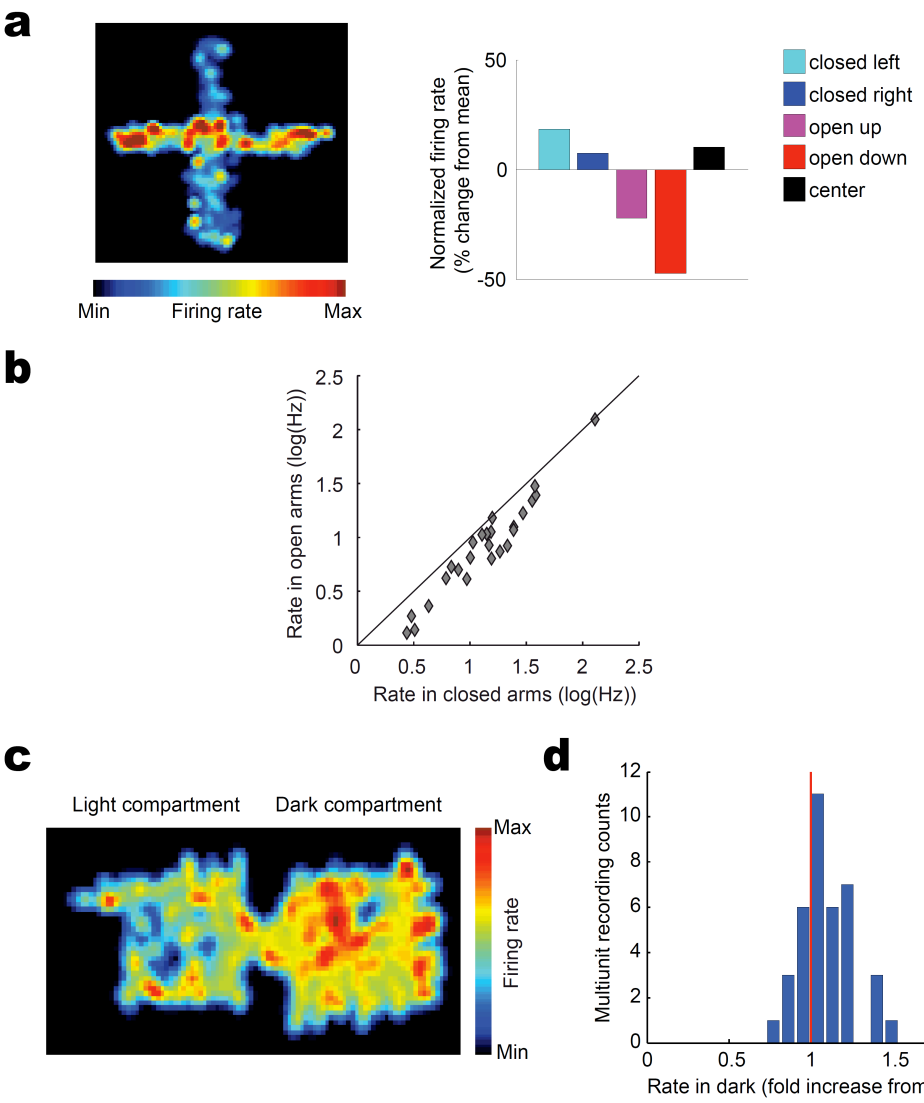

Supplementary Figure 19. adBNST multiunit activity is higher in the safe compartments of anxiety paradigms.

Mice were implanted with a drivable microdrive containing 8 stereotrodes in the adBNST to allow recording of adBNST multiunit activity. Mice were run in the EPM **(a-b)** and the light-dark box **(c-d)**. **(a)** Spatial firing rate map (left) and normalized firing rates (% difference from mean rate) from each arm are shown for a representative multiunit recording in the adBNST of a mouse exploring the EPM for 15 min. Note that activity is higher on both closed arms of the maze. Left: warmer colors correspond to higher firing rates. **(b)** Scatterplot showing rate in the closed arms and in the open arms for all multiunit recordings (*n* = 32 multiunit recordings from 4 mice). Rates were significantly higher in closed arms ($p<10^{-5}$, Wilcoxon signed-rank test). Note that adBNST multiunit activity from all channels in all mice was higher in the closed arms. Data were plotted as natural logarithm transforms of raw firing rates in Hz to allow for easier visualization. **(c)** Spatial firing rate map of a representative multiunit recording in the adBNST of a mouse exploring the light dark test for 15 minutes. Note that activity is higher in the dark compartment of the light-dark test box. The protrusion on the upper corner of the left chamber was caused by the position tracking LED reflecting off one of the walls. Warmer colors represent higher firing rates. **(d)** Histogram of multiunit firing rate in the dark compartment plotted as fold-increase from the light compartment. Note that the mean of this distribution is significantly higher than 1 (mean =1.16, $p<0.005$, Wilcoxon signed-rank test).

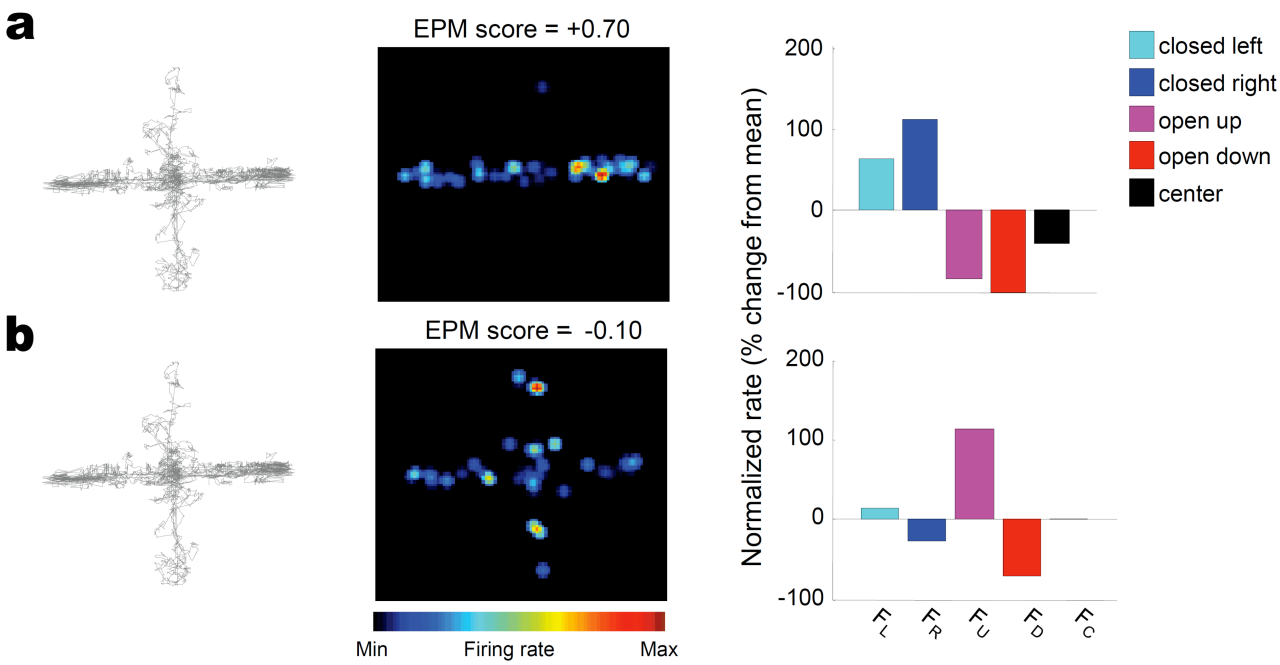

$$\text{EPM score} = (A - B) / (A + B), \text{ where}$$

$$A = 0.25 * (|F_L - F_U| + |F_L - F_D| + |F_R - F_U| + |F_R - F_D|) \text{ and}$$

$$B = 0.5 * (|F_L - F_R| + |F_U - F_D|)$$

Supplementary Figure 20. Calculation of EPM scores to measure differentiation between closed and open arms by adBNST single units.

Two representative single units from the same mouse were recorded simultaneously during a 15-min EPM exploration session. **(a)** Left panel: behavioral track showing the path taken by the mouse in the EPM. Middle panel: spatial firing rate map for a single unit that differentiated closed and open arms (higher rates are indicated by warmer colors). This unit was more active in the closed arms. Right panel: Bar graph showing normalized firing rates (plotted as % change from mean rate) for each sub-location in the EPM. Note that this unit fired more in both closed arms. The EPM score of this unit, which was calculated according to the formula below the figure, is displayed above its spatial firing rate map. F_L, F_R, F_U, F_D and F_C indicate, respectively normalized firing rates (% change from mean rate) in the left arm, right arm, up arm, down arm and center of the EPM. **(b)** Same as **(a)**, but for a single unit recorded in the same session that did not display task-related activity in the EPM. Note that although the unit fired differently in different arms, the unit did not consistently differentiate closed arms from open arms, resulting in a low EPM score (see Supplementary Methods). In contrast, a high EPM score indicates that a unit has similar firing rates in arms of the same type and different firing rates in arms of different types. The unit in **(a)** has similar firing rates in arms of the same type, but closed and open rates are very different from each other.

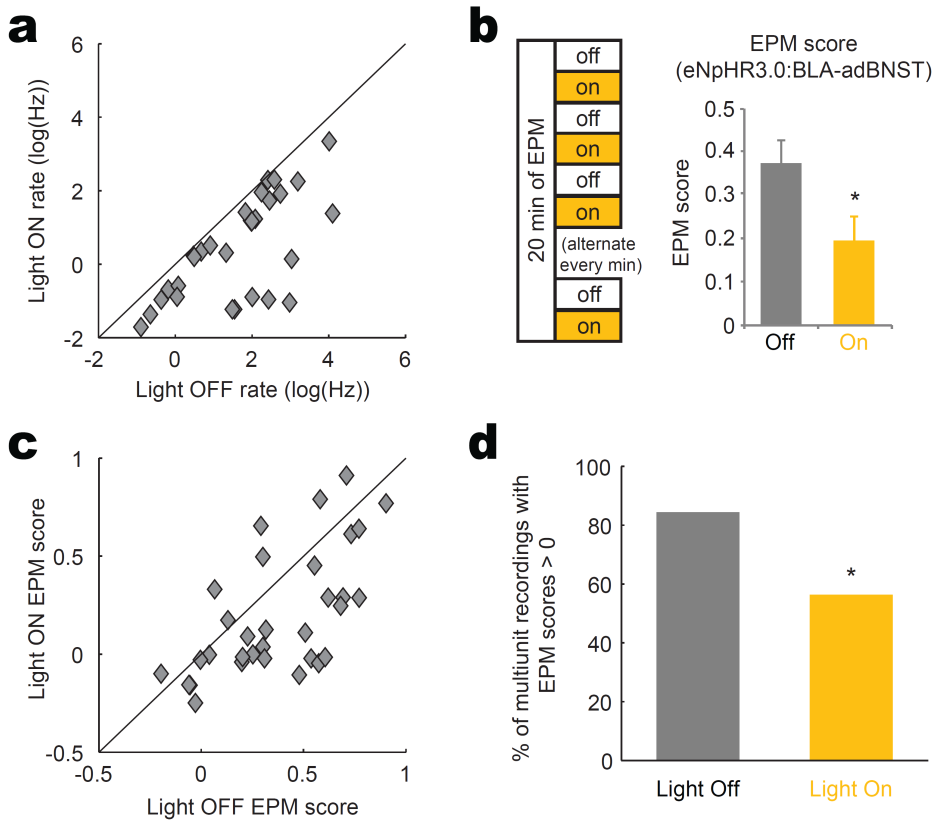

Supplementary Figure 21. adBNST multiunit activity depends on BLA inputs to differentiate safe and aversive locations on the EPM.

(a) Scatterplot of multiunit firing rates during yellow light OFF and ON epochs in eNpHR3.0:BLA-adBNST mice. **(b)** eNpHR3.0:BLA-adBNST mice were run in the EPM for 20 minutes with alternating 1-min laser-off and laser-on epochs (same experiment as **Fig. 4**). Inhibition of the BLA-adBNST projection decreased the EPM score of multiunit recordings (*n* = 32 recordings, $p<0.05$, Wilcoxon signed-rank test), in agreement with single-unit data. Values are mean ± s.e.m. **(c)** Scatterplot showing the distribution of EPM score changes. 25/32 recordings showed lower EPM scores in the light ON compared to the OFF epoch. EPM scores were significantly higher in the light OFF epoch ($p<0.01$, Wilcoxon signed-rank test). **(d)** The number of multiunit recordings with positive EPM scores also decreased with yellow light ($p < 0.05$, Fisher's exact test).

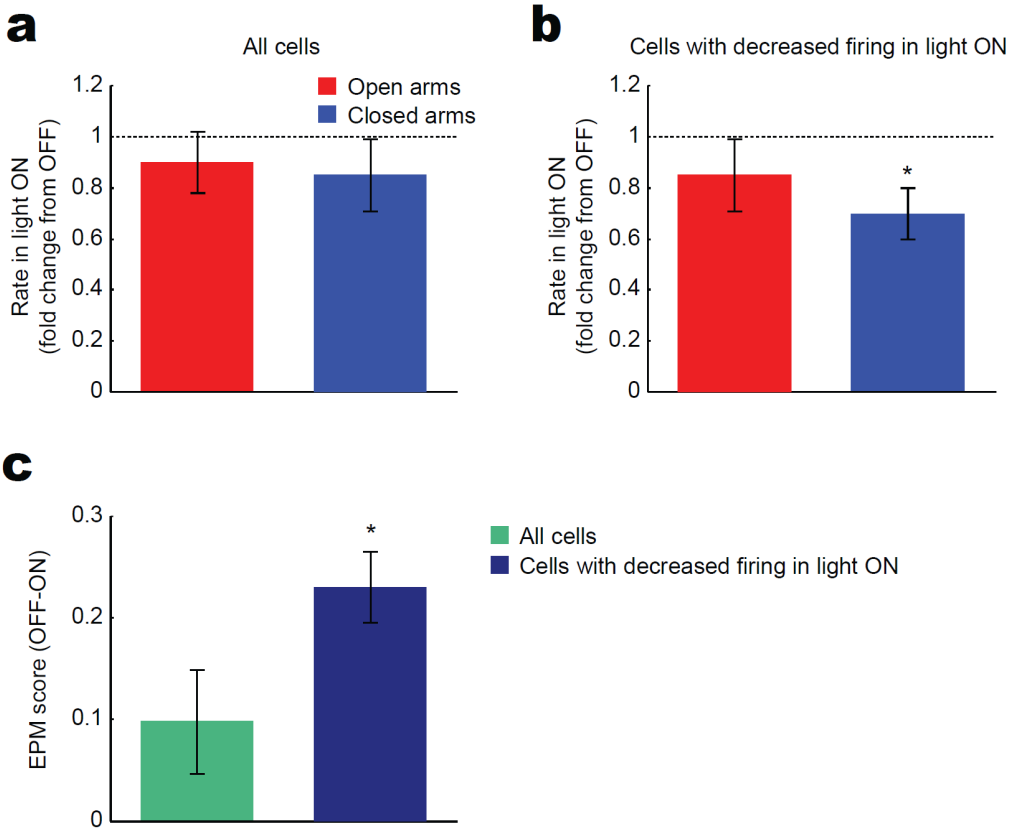

Supplementary Figure 22. Inhibiting the BLA-adBNST projection decreases firing rates in the closed arms and EPM scores.

eNpHR3.0:BLA-adBNST mice were run in the EPM for 20 minutes with alternating 1-min laser-off and laser-on epochs (same experiment as **Fig. 4**). **(a)** Inhibiting the BLA-adBNST projection tended to decrease firing rates of adBNST single units, but this effect did not reach statistical significance when pooling all neurons together ($p<0.68$, Wilcoxon's test, n = 38 single units from 4 mice). **(b)** However, the adBNST single units that exhibited a significant decrease in firing rate during light ON epochs (n = 20 out of 38 single units) displayed a significant decrease in rate in the closed arms ($p<0.05$, Wilcoxon signed-rank test), but not in the open arms ($p<0.34$, Wilcoxon signed-rank test). Significance of light-induced decreases in firing were tested by comparing rates across 10 one minute-long light OFF and 10 light ON epochs for each single unit. **(c)** Decreases in EPM scores were higher in adBNST single units with significant decreases in firing rate during light ON (n = 38 for all cells, n = 20 for cells with decreased firing in light ON, $p<0.05$, Wilcoxon signed rank test). Values are mean ± s.e.m.

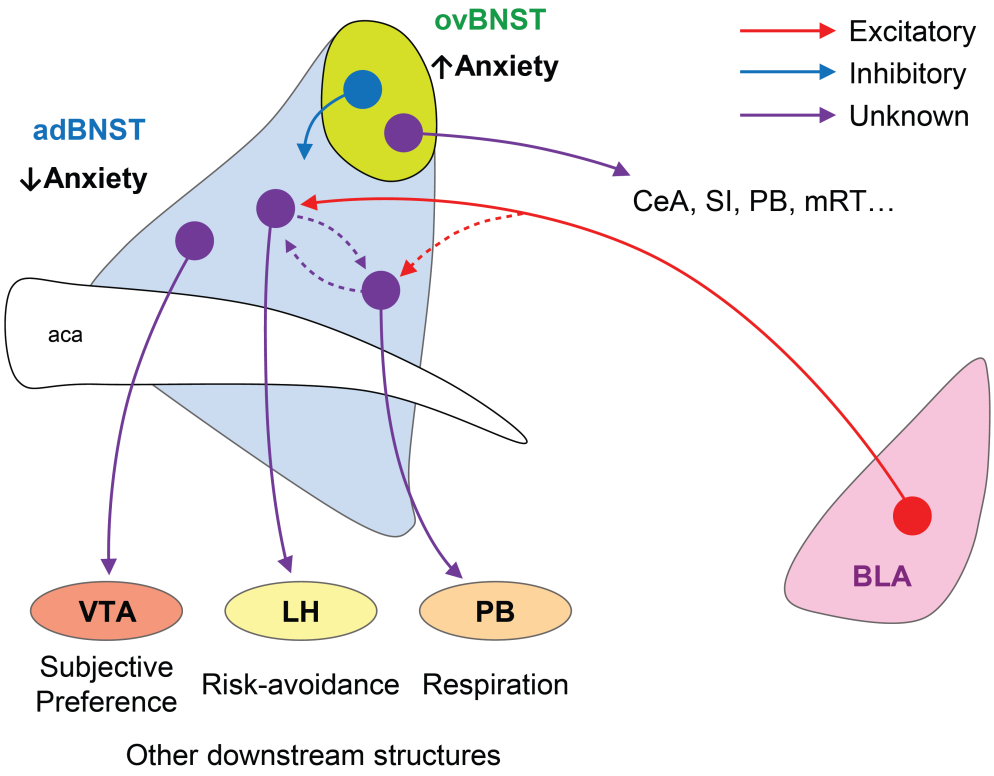

Supplementary Figure 23. Summary diagram

Schematic illustrating possible functional organization of BNST circuitry. The ovBNST inhibits the adBNST, whereas the adBNST sends only a weak projection to the ovBNST. The adBNST projects to the LH, PB and VTA. Each of these projections decrease distinct aspects of anxiety expression. The coordinated recruitment of these subpopulations may be implemented by recurrent circuitry in adBNST. BLA inputs likely recruits BNST output neurons to LH and PB, but not VTA in certain circumstances. The ovBNST may act to increase anxiety by inhibiting the adBNST or by independently influencing downstream structures, such as the central amygdala (CeA), substantia innominata (SI), PB or mesencephalic reticular formation (mRT). Red and blue arrows indicate excitatory and inhibitory projections, respectively. Purple arrows indicate projections with unknown neurotransmitter identity. Solid lines indicate the projections directly targeted and investigated in this study, and dashed lines indicate the projections suggested to exist by the data.

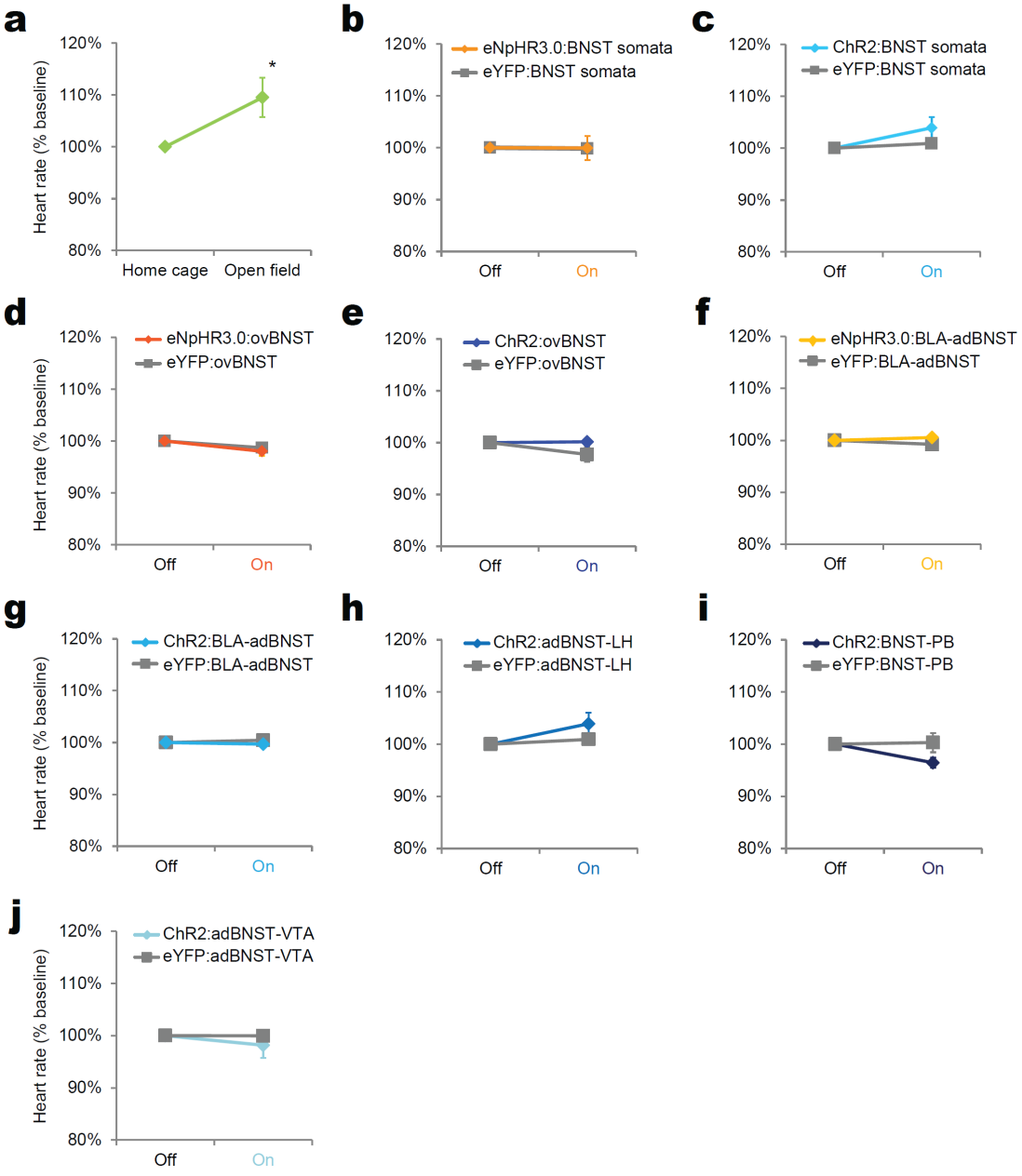

Supplementary Figure 24. Heart rate was not altered in any of the optogenetic manipulations performed.

(a) Heart rate was significantly increased by placing the animals into an open field apparatus, an anxiogenic environment, compared to the values measured in the home cage (n = 7; $p < 0.01$). However, **(b)** inhibiting the BNST somata (n = 7 for exp; n = 8 for controls; $p > 0.05$), **(c)** stimulating the BNST somata (n = 6 for exp; n = 6 for controls; $p > 0.05$), **(d)** inhibiting the ovBNST (n = 8 for exp; n = 8 for controls; $p > 0.05$), **(e)** stimulating the ovBNST (n = 7 for exp; n = 7 for controls; $p > 0.05$), **(f)** inhibiting BLA fibers in the adBNST (n = 7 for exp; n = 7 for controls; $p > 0.05$), **(g)** stimulating BLA fibers in the adBNST (n = 7 for exp; n = 8 for controls; $p > 0.05$), **(h)** stimulating adBNST fibers in the LH (n = 9 for exp; n = 9 for controls; $p > 0.05$), **(i)** stimulating BNST fibers in the PB (n = 8 for exp; n = 7 for controls; $p = 0.12$), or **(j)** stimulating adBNST fibers in the VTA (n = 8 for exp; n = 7 for controls; $p > 0.05$) had no detectable effect on heart rate. Values are mean ± s.e.m.